AGU PUBLICATIONS

JGR

Journal of Geophysical Research: Oceans

RESEARCH ARTICLE

10.1002/2013JC009722

Key Points:
- Just seaward of the surfzone, mixing is reduced to deep ocean diffusivities
- Transient rip current ejections dominate surfzone/inner-shelf tracer exchange
- At long times, shoreline-released dye recycles from inner-shelf back to surfzone

Correspondence to:
K. Hally-Rosendahl,
kai@coast.ucsd.edu

Citation:
Hally-Rosendahl, K., F. Feddersen, and R. T. Guza (2014), Cross-shore tracer exchange between the surfzone and inner-shelf, *J. Geophys. Res. Oceans*, *119*, doi:10.1002/2013JC009722.

Received 10 DEC 2013
Accepted 8 MAY 2014
Accepted article online 14 MAY 2014

Cross-shore tracer exchange between the surfzone and inner-shelf

Kai Hally-Rosendahl[1], Falk Feddersen[1], and R. T. Guza[1]

[1]Integrative Oceanography Division, Scripps Institution of Oceanography, UCSD, La Jolla, California, USA

Abstract Cross-shore tracer exchange between the surfzone and inner-shelf is examined using temperature and dye measurements at an approximately alongshore-uniform beach. An alongshore-oriented plume is created by releasing dye continuously for 4.5 h in a surfzone alongshore current. The plume is sampled for 13 h from the release point to 700 m downstream, between the shoreline and 250 m offshore (6 m water depth). Within the surfzone ($\leq$2 m depth), water is relatively warm, and dye is vertically well mixed. On the inner-shelf (3–6 m depth), alongshore currents are weak, and elevated temperature and dye co-occur in 25–50 m wide alongshore patches. Within the patches, dye is approximately depth-uniform in the warm upper 3 m where thermal stratification is weak, but decreases rapidly below 3 m with a strong thermocline. Dye and temperature vertical gradients are correlated, and dye is not observed below 18 °C. The observations and a model indicate that, just seaward of the surfzone, thermal stratification inhibits vertical mixing to magnitudes similar to those in the ocean interior. Similar surfzone and inner-shelf mean alongshore dye dilution rates are consistent with inner-shelf dye properties being determined by local cross-shore advection. The alongshore-patchy and warm inner-shelf dye is ejected from the surfzone by transient rip currents. Estimated Stokes drift driven cross-shore exchange is small. The transient rip current driven depth-normalized heat flux out of the surfzone has magnitude similar to those of larger-scale shelf processes. Dye recycling, from the inner-shelf back to the surfzone, is suggested by relatively long surfzone dye residence times.

1. Introduction

The surfzone (the region between the shoreline and the seaward boundary of depth-limited wave breaking) and the inner-shelf (extending seaward from the surfzone to nominally 20 m water depth) are widely used for recreation and commerce, and are important habitats for larvae and other marine organisms [e.g., *McLachlan and Brown*, 2010]. Surfzone and inner-shelf water quality is often compromised by contaminants from terrestrial runoff and offshore waste disposal [e.g., *Koh and Brooks*, 1975; *Schiff et al.*, 2000]. Tracers (pollutants, sediment, larvae, etc.) with shoreline sources are first mixed and transported within the surfzone [e.g., *Harris et al.*, 1963; *Inman et al.*, 1971; *Grant et al.*, 2005; *Clark et al.*, 2010], and ultimately diluted by exchange with the inner-shelf. Conversely, tracers on the inner-shelf can be transported into the surfzone [e.g., *Boehm et al.*, 2002; *Noble et al.*, 2009; *Wong et al.*, 2012]. The surfzone and inner-shelf are each dynamically complex, with very different processes driving dispersion. The intersection of, and exchange between, these two regions is not understood.

Dye tracers and Lagrangian surface drifters have been used recently to observe nearshore dispersion. *Clark et al.* [2010] studied the cross-shore dispersion of a dye tracer continuously released in the surfzone at alongshore-uniform Huntington Beach, California. However, observations were limited to $\leq$2 h and usually $<$400 m downstream of the dye source, and analyses were specifically restricted to the surfzone-contained portions of the dye plumes. *Spydell et al.* [2007, 2009] observed Lagrangian drifter dispersion at alongshore-uniform beaches, but analysis periods were limited to $<$17 min, when drifters were generally surfzone confined.

Several mechanisms, spanning a range of time and length scales, can drive cross-shore exchange across the inner-shelf and the surfzone. In 12 m water depth with small waves, cross-shelf winds can drive subtidal cross-shore exchange on the inner-shelf [e.g., *Fewings et al.*, 2008]. Along-shelf winds are less effective than cross-shelf winds in driving cross-shore inner-shelf exchange at subtidal time scales [e.g., *Austin and Lentz*, 2002; *Kirincich et al.*, 2009]. In Southern California, the site of the present observations, internal tides and higher frequency internal waves can drive cross-shore exchange. Semidiurnal internal tides in 20 m depth

can cause significant cross-shore heat and nitrate fluxes [*Lucas et al*., 2011]. Diurnal and semidiurnal internal tides can advect cold water from 60 m depth several km onshore to less than 6 m depth [*Boehm et al*., 2002]. Higher frequency internal bores can propagate into shallow depths (5 m) and cause minute-to-hour fluctuations in temperature [*Winant*, 1974; *Pineda*, 1991, 1994] and phytoplankton [*Omand et al*., 2011].

In water depths less than about 15 m when waves are significant, cross-shore flow can be dominated by surface gravity wave forcing, even with no wave breaking [*Lentz et al*., 2008; *Fewings et al*., 2008]. With weak vertical mixing, the offshore Eulerian flow is roughly equal in magnitude but opposite in direction to the onshore Stokes drift at all depths, resulting in no cross-shore exchange. However, with strong vertical mixing, the mismatch in vertical structures of the onshore Stokes flow and offshore Eulerian flow can induce significant cross-shore exchange [e.g., *Lentz et al*., 2008; *Kirincich et al*., 2009]. Surface gravity wave conditions often vary over periods of a few days, so this wave-driven exchange mechanism varies on subtidal time scales.

Surfzone wave breaking drives currents and eddies that can lead to rip currents, long-recognized to exchange water between the surfzone and inner-shelf [e.g., *Inman et al*., 1971; *Talbot and Bate*, 1987, among others]. Most observational rip current studies have focused on beaches with alongshore inhomogeneous bathymetry, with rips located near channels in sand bars. Bathymetrically controlled rips can vary temporally, often pulsing on infragravity time scales [e.g., *MacMahan et al*., 2004]. *Smith and Largier* [1995] observed reoccurring rip currents near a pier, possibly bathymetrically controlled, and inferred that these rips dominated the exchange between the surfzone and inner-shelf. On beaches with alongshore-uniform bathymetry and no solid structures (e.g., piers or jetties), rip currents are often temporally transient and lack preferred alongshore locations. Transient rips eject seaward the vorticity (eddies) generated in the surfzone by finite crest length wave breaking [*Peregrine*, 1998; *Clark et al*., 2012], but their time and length scales are not well understood [*Johnson and Pattiaratchi*, 2006]. Infrared remote sensing of ocean surface temperature [*Marmorino et al*., 2013] and X-band radar backscatter [*Haller et al*., 2014] can reveal these ejection events. Surfzone flushing by bathymetrically controlled rip currents has been estimated to occur in a few hours, but most of the flushed water returns to the surfzone [*Reniers et al*., 2009; *MacMahan et al*., 2010]. Similarly, over a few hours, surfzone-released dye tracer [*Clark et al*., 2010] and surface drifters [*Spydell et al*., 2009] at alongshore-uniform beaches are observed to generally remain within two surfzone widths (≈100–200 m during these studies) of the shoreline.

Vigorous vertical mixing in the surfzone [*Feddersen and Trowbridge*, 2005; *Ruessink*, 2010; *Feddersen*, 2012a] suggests there will be at most weak vertical structure in surfzone temperature or dye concentration. However, significant inner-shelf stratification ($\approx 0.7\,^{\circ}\mathrm{C\ m^{-1}}$) has been observed just offshore (≈5 m water depth) of Southern California surfzones in late summer and early fall [*Winant*, 1974; *Omand et al*., 2011]. We show that this stratification can play an important role in surfzone/inner-shelf exchange.

Cross-shore tracer exchange between the surfzone and the inner-shelf was observed during the multidisciplinary IB09 experiment conducted at alongshore-uniform Imperial Beach, California. Extensive temperature and dye measurements were made with novel and complimentary instrument platforms. Temperature is a dynamical tracer with multiple sources and sinks (e.g., solar heating, air-sea fluxes), whereas dye is a passive tracer with a known and localized source. These unique, coupled observations resolve tracer structure and evolution in both the surfzone and inner-shelf, and in the cross-shore, alongshore, and vertical directions.

The IB09 experiment site, dye release method, instrument platforms, and sampling schemes are described in section 2. Background waves and currents are discussed in section 3.1. In section 3.2, overviews of dye and temperature observations are given, and time periods for subsequent analyses established. The cross-shore and vertical structures of dye and temperature in the surfzone and inner-shelf are described in sections 3.3 and 3.4. Alongshore and vertical inner-shelf tracer structure is analyzed in section 3.5. The relationship between dye concentration and temperature in both the surfzone and inner-shelf is examined in section 3.6. Cross-shore and alongshore dye dilution is examined in section 3.7, and surfzone alongshore dye transport estimates are presented in section 3.8. Results are synthesized in section 4. In particular, inner-shelf vertical tracer mixing (section 4.1), the magnitude and mechanisms of cross-shore surfzone/inner-shelf tracer exchange (section 4.2), and the implications of these observations for surfzone dilution modeling (section 4.3) are discussed. Section 5 is a summary.

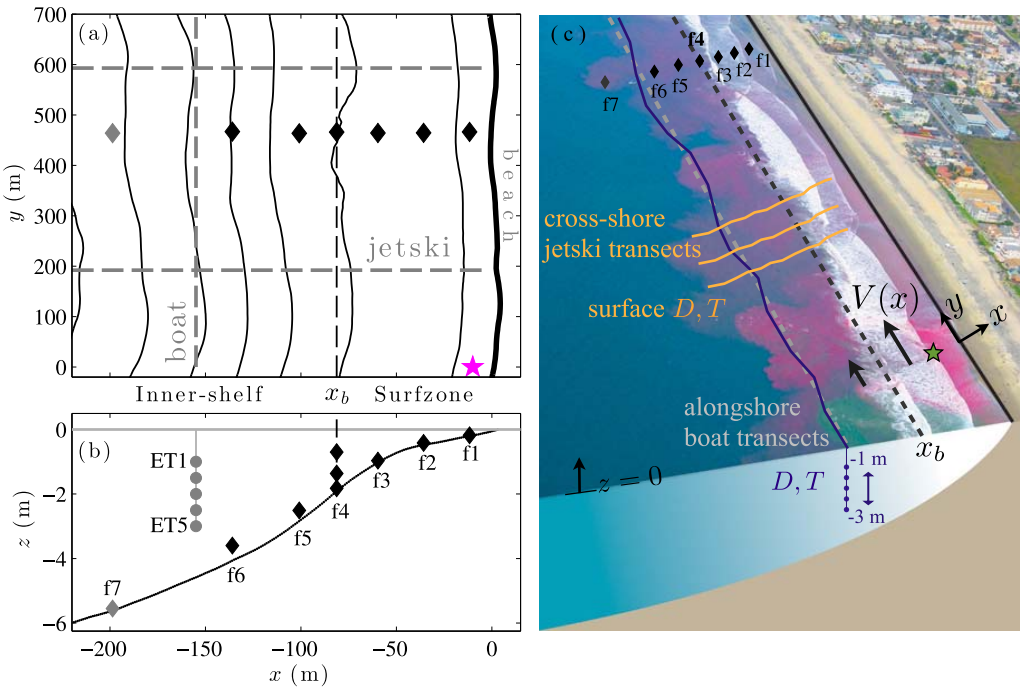

Figure 1. (a) Plan view of IB09 bathymetry contours versus cross-shore coordinate x and alongshore coordinate y. Star indicates dye release location. Diamonds denote the cross-shore array of instrumented frames f1–f7. Vertical, black dashed line through f4 denotes the seaward surfzone boundary x_b, defining the surfzone ($x \geq x_b$) and the inner-shelf ($x < x_b$). Vertical, gray dashed line at $2x_b$ is an idealized alongshore boat transect. Horizontal, gray dashed lines ($y = 200$, 600 m) represent idealized cross-shore transects driven repeatedly by jet-skis at various alongshore locations. (b) Depth h (curve) versus cross-shore coordinate x, with mean sea level at $z = 0$ m. Diamonds are f1–f7 locations; f4 is instrumented at three vertical locations. The mean cross-shore location of the alongshore-towed vertical array ET1-ET5 (circles) is at $2x_b$. Waves, currents, dye, and temperature are measured at f1–f6 (black symbols), whereas only dye and temperature are measured at f7 and ET1-ET5 (gray symbols). (c) A 29 September 2009 aerial photograph with superposed coordinate system (x, y, z), mean alongshore current V, surfzone boundary x_b, mean cross-shore location of inner-shelf alongshore boat transects ($2x_b$), dye release location (star), and instrument frames (f1–f7). Dye is alongshore-patchy on the inner-shelf.

2. IB09 Experiment

2.1. Field Site and Coordinate System

IB09 field observations were acquired during fall 2009 at Imperial Beach, California (32.6°N, 117.1°W), a west (269.6°) facing beach with an approximately straight shoreline (Figure 1). The case study presented here is 11:00–24:00 h (PDT) on 29 September 2009. In the right-handed coordinate system, cross-shore coordinate x increases negatively seaward ($x = 0$ m at the mean shoreline), alongshore coordinate y increases positively toward the north ($y = 0$ m at the dye release location), and vertical coordinate z increases positively upward ($z = 0$ at mean sea level, Figure 1). Bathymetry surveys from 25 September to 2 October were similar, and are averaged to give a representative bathymetry for 29 September that is approximately alongshore-uniform (Figures 1a and 1b). 29 September wind, measured at a nearby meteorological station, was light onshore (approximately 4–9 knots, WNW), typical for Southern California.

2.2. Dye Release

Rhodamine WT dye (2.1×10^8 parts per billion (ppb)) was released continuously into the surfzone near the shoreline at $(x, y) = (-10, 0)$ m at 3.6 mL s^{-1} for approximately 4.5 h (11:10–15:47 h). A peristaltic pump atop a heavy metal cart forced the dye through a small hose and out of a diffuser roughly 20 cm below the surface. Visual observations suggested rapid vertical mixing, and measured surface dye concentrations were reduced from $O(10^8)$ ppb to less than 100 ppb within 10 m of the release. Therefore, the initially concentrated dye (1.2 specific gravity) was quickly diluted to a specific gravity of approximately 1. Rhodamine WT has a photochemical decay e-folding time of approximately 667 h of sunlight [e.g., *Smart and Laidlaw*, 1977]. Therefore, photochemical decay over the approximately 8 h of sunlight during this study is negligible.

2.3. Surfzone and Inner-Shelf Instrumentation

2.3.1. Cross-Shore Array

A 190 m long cross-shore array of seven fixed, near-bed instrument frames (denoted f1–f7, onshore to offshore) was deployed from near the shoreline to approximately 6 m water depth, 465 m north of the 29 September dye release location (diamonds, Figures 1b and 1c). Frames f1–f6 held Paros pressure sensors and SonTek acoustic Doppler velocimeters (ADVs) to measure waves and currents, Yellow Springs Instrument Company thermistors to measure temperature T, and WET Labs ECO Triplet fluorometers (hereafter ET) to measure dye concentration D. One frame (f4), located near the seaward edge of the surfzone (2.1 m water depth), held instrument packages at three locations spanning 1.1 m vertically (0.2, 0.7, and 1.3 m above the bed). Instruments on frames f1–f6 sampled for 51 min each hour. The remaining 9 min of each hour were used by the ADVs to estimate the bed location. Frame f7 held a thermistor-equipped ET to measure temperature and dye concentration. The ET on f7 sampled from 11:00 to 17:30 h, whereas f1–f6 instruments sampled throughout the entire day.

2.3.2. Surface Dye and Temperature Cross-Shore Transects

Surface T and D were measured with thermistors and fluorometers mounted on two GPS-tracked jetskis [*Clark et al*., 2009] that drove repeated cross-shore transects from $x \approx -250$ m to the shoreline (Figures 1a and 1c) between $y = 0$ m and $y = 600$ m. The alongshore spacing between transects varied from approximately 20 to 200 m. Outbound transects, sometimes corrupted when the jetskis swerved or became airborne jumping over waves, are discarded. Inbound transects, when jetskis were driven immediately in front of bores to minimize turbidity from bubbles and suspended sand, are analyzed during 11:10–16:00 h.

2.3.3. Inner-Shelf Dye and Temperature Alongshore Transects and CTD+F Casts

Offshore of the surfzone, the alongshore and vertical structure of dye concentration $D(y,z)$ and temperature $T(y,z)$ was measured with a vertical array of five thermistor-equipped ETs towed alongshore behind a small boat. The vertical array sampled from $z = -1$ to -3 m at 0.5 m spacing (Figure 1b). During approximately 11:00–16:00 h, repeated ≈700 m long alongshore transects were driven at roughly 0.7 m s^{-1} at a mean cross-shore location nominally twice the surfzone width. The transects were approximately shore-parallel with deviations to avoid large waves (e.g., Figure 2a).

The inner-shelf vertical structures of T and D were also measured with small boat CTD+F casts using a Seabird SBE25 CTD and colocated WET Labs Rhodamine WT fluorometer. Casts extended from near the surface to the seabed in approximately 4–6 m water depth. Analyses include 21 casts during 11:49–15:17 h within dye plumes located $-313 \le x \le -141$ m, $-338 \le y \le 592$ m. CTD salinity varied <0.2 psu, consistent with weak salinity variations observed over the upper water column 30 km to the north [*Lucas et al*., 2011] and at the SIO pier (≈40 km to the north, sccoos.org).

2.4. Corrections to Measured Dye Fluorescence

Rhodamine WT fluorescence is temperature dependent [*Smart and Laidlaw*, 1977], and measured fluorescence depends on the turbidity (e.g., from sand and bubbles) of the sample [*Clark et al*., 2009]. All D observations are corrected for temperature [*Smart and Laidlaw*, 1977], and all D observations except those from the CTD+F casts (where turbidity measurements are not available) are corrected for turbidity [*Clark et al*., 2009]. Corrected D typically differ from measured D by less than 5%.

2.5. Dye and Temperature Averaging

Depending on the situation, temperature and dye concentration are averaged over time, cross-shore direction, alongshore direction, vertical direction, or realizations (jetski transects, boat transects, and CTD+F casts). Throughout, temperature statistics are computed arithmetically. Since dye concentration is a positive semidefinite quantity, dye statistics are at times computed logarithmically, such that mean dye concentration $\bar{D} = \exp[E(\log D)]$, where $E()$ represents the typical averaging operator (expected value). The logarithmically computed dye concentration standard error is defined as $\bar{D} \pm \sigma_D = \exp[E(\log D) \pm \mathrm{std}(\log D)]$, where $\bar{D} \pm \sigma_D$ represents ± a standard deviation from the mean, ensuring that $\bar{D} - \sigma_D \ge 0$. Figure captions indicate when dye statistics are computed logarithmically.

3. Results

3.1. Background Waves and Alongshore Currents

The bathymetry is terraced close to shore ($x > -40$ m), and approximately planar (slope ≈ 0.02) farther offshore (Figure 3c). The average (11:00–16:00 h) significant wave height $H_s(x)$ shoals to a maximum of 0.71 m

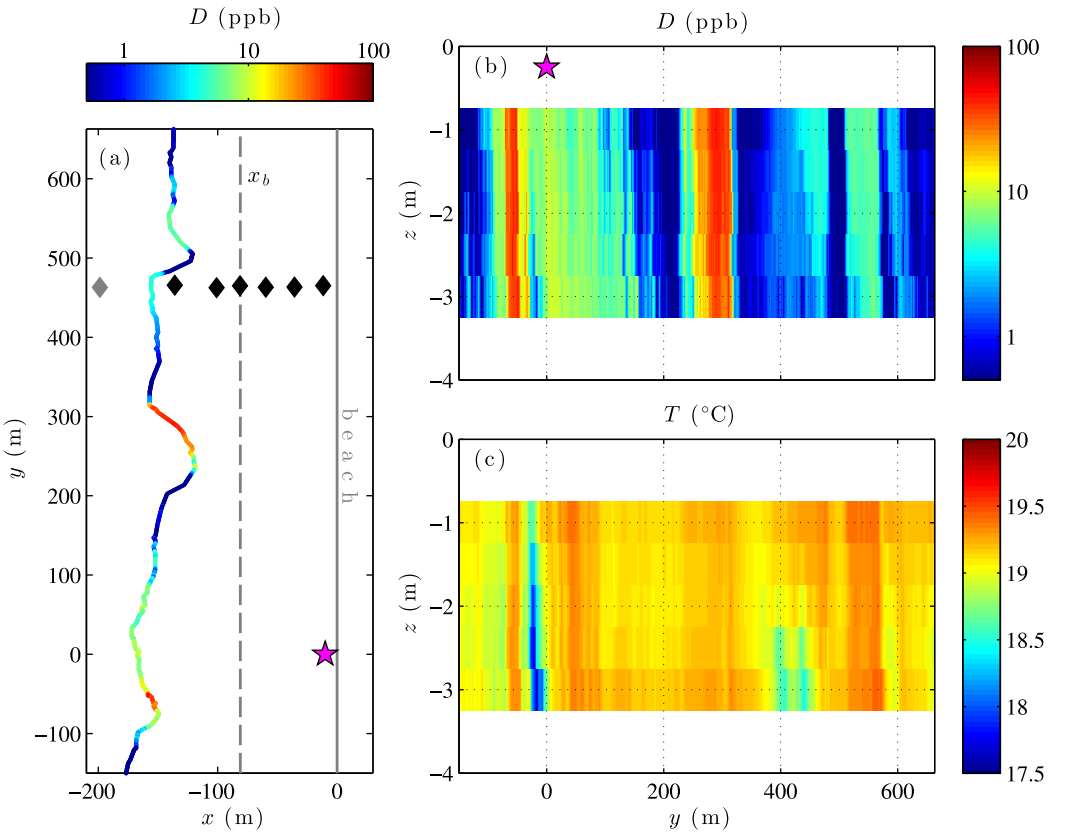

Figure 2. (a) Dye concentration D at $z=-2$ m versus cross-shore coordinate x and alongshore coordinate y from an alongshore boat transect ($t \approx$ 12:40–13:00 h). Magenta star denotes the dye release location, dashed line the surfzone boundary x_b, and diamonds the bottom-mounted frames f1–f7. (b) Dye concentration D and (c) temperature T versus alongshore coordinate y and vertical coordinate z. Star in Figure 2b denotes the alongshore and vertical location of the shoreline-released dye.

near f4 ($x=-81$ m), and then decreases shoreward after waves break (Figure 3a). The incident wave peak period is $T_p = 14$ s. The mean (11:00–16:00 h) alongshore current $V(x)$ is northward (positive) at all locations, with a maximum (0.17 m s^{-1}) inside the surfzone near f2 (Figure 3b). The 5 min averaged alongshore current fluctuates at very low frequencies (bars in Figure 3b), but is always northward within the surfzone. At f4, the vertical variation of V is weak (compare shaded symbols in Figure 3b). Seaward of the surfzone, the mean alongshore current weakens; $V = 0.06$ and 0.02 m s^{-1} at f5 and f6, respectively.

During 11:00–16:00 h, the incident wavefield is relatively constant, and the tide varies by only 0.35 m (low tide is at 13:27 h, Figure 4a). Hourly cross-shore profiles of H_s and V vary little, and for this time period the seaward surfzone boundary is defined as the f4 cross-shore location, $x_b = -81$ m (mean depth $h_b = 2.1$ m, Figure 3c).

3.2. Time Variation of Bulk Dye and Temperature

Surfzone bulk temperature $\langle T \rangle$ and dye concentration $\langle D \rangle$ are calculated as 30 min averages, integrated over the surfzone frames f1–f4 (curves in Figures 4b and 4c). The mean vertical location of f1–f4 is $z \approx -1$ m. Inner-shelf $\langle T \rangle$ and $\langle D \rangle$ (nominally at $2x_b$) are calculated at ET1 ($z = -1$ m), averaged over each alongshore boat transect (dots in Figures 4b and 4c). Vertical variation is described in sections 3.4 and 3.5.

The dye release begins at 11:10 h (magenta bar in Figure 4c). Prior to 13:00 h, the surfzone is warmer, and warms more rapidly, than the inner-shelf (Figure 4b), due in part to the greater efficacy of solar heating in the shallower surfzone. The surfzone/inner-shelf $\langle T \rangle$ difference increases from 0.15 °C to 0.33 °C. This differential surfzone and inner-shelf warming is discussed in section 4.2. From 11:10 to 13:00 h, $\langle D \rangle$ is not steady, increasing in both the surfzone and inner-shelf (Figure 4c). After 13:00 h, a fog bank decreases incident solar radiation significantly, the surfzone cools, and surfzone and inner-shelf $\langle T \rangle$ equilibrate (Figure 4b). Between

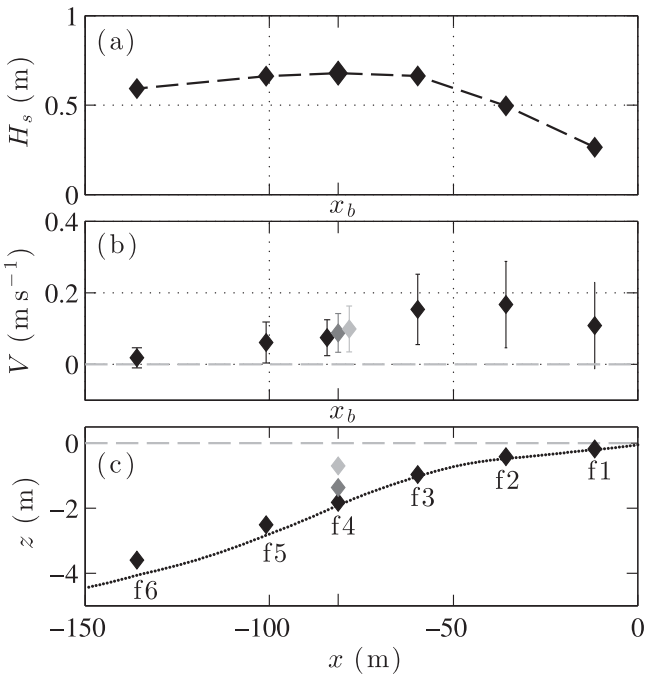

Figure 3. Time-averaged (11:00–16:00 h) (a) significant wave height H_s, (b) alongshore current V, and (c) vertical locations of f1–f6 versus cross-shore coordinate x. Seaward surfzone boundary x_b is the cross-shore location of maximal H_s (f4). In Figure 3b, vertical bars indicate standard deviations of 5 min averaged alongshore velocities. In Figure 3c, the black curve gives the bathymetry $h(x)$.

13:00 and 16:00 h, surfzone and inner-shelf bulk dye concentrations are approximately stationary (Figure 4c).

The time variation in $\langle T \rangle$ and $\langle D \rangle$ motivates defining two separate analysis periods (shaded regions in Figure 4). The first time period SC (for secular change) is 11:10–13:00 h, when surfzone and inner-shelf $\langle T \rangle$ and $\langle D \rangle$ increase (Figures 4b and 4c). The second time period EQ (for equilibration) is 14:00-16:00 h, when $\langle T \rangle$ and $\langle D \rangle$ are approximately stationary (Figures 4b and 4c). These two time periods will often be analyzed separately.

3.3. Cross-Shore Structure of Dye and Temperature: Surfzone and Inner-Shelf

Surface mean temperature $\bar{T}(x)$ and dye concentration $\bar{D}(x)$ for SC and EQ are calculated by time- and alongshore-averaging ($0 < y < 600$ m) all cross-shore jetski transect realizations during each period (Figure 5). These jetski surface observations are qualitatively consistent with the $z \approx -1$ m bulk quantities calculated using the surfzone frames and inner-shelf alongshore boat transects (section 3.2).

During SC, surface $\bar{T}(x)$ has a surfzone maximum (19.28 °C at $x = -30$ m) and decreases to a minimum near $2x_b$ on the inner-shelf (Figure 5a, blue). The cross-shore surface temperature difference of $\bar{T}_{\max} - \bar{T}_{\min} = 0.14$ °C is similar to the mean SC surfzone to inner-shelf bulk temperature difference $\Delta\langle T \rangle_{SZ-IS} = 0.25$ °C (Figure 4b). During EQ, surface $\bar{T}(x)$ is warmer than during SC at all x (with $\bar{T}_{\max} = 19.48$ °C) and is nearly cross-shore uniform (Figure 5a, red), consistent with the 14:00–16:00 h surfzone and inner-shelf $\langle T \rangle$ equilibration (Figure 4b). Surface T increases steadily during SC, so the variance is larger than during EQ (compare blue and red vertical bars in Figure 5a).

Although dye is nonstationary during SC, surface $\bar{D}(x)$ has a similar profile shape during SC and EQ, with a surfzone maximum and monotonic decrease offshore (Figure 5b). Consistent with the surfzone and inner-shelf $\langle D \rangle$ (Figure 4c), surface $\bar{D}(x)$ is greater at all x during EQ than SC, D variability is smaller during EQ than SC, surfzone $\bar{D}(x)$ is more cross-shore uniform during EQ than SC, and EQ surface $\bar{D}(2x_b) \approx 0.4\bar{D}(x_b)$ (Figure 5b).

During SC and EQ, time-averaged temperature $\bar{T}(x,z)$ at the fixed cross-shore array ($y = 465$ m) is warm and roughly uniform within and near the surfzone (f1–f5, Figures 6a and 6c). However, $\bar{T}(x,z)$ decreases significantly at the deeper frames; $\bar{T} \approx 18.5$ °C at $(x,z)_{f6} = (-135, -3.6)$ m, and $\bar{T} \approx 17.1$ °C at $(x,z)_{f7} = (-199, -5.7)$ m (Figures 6a and 6c). In contrast, the jetski-measured surface temperature varies much less in the cross-shore during each period, with variations of less than 0.2 °C between the shoreline and $x = -230$ m (Figure 5a). Vertical temperature stratification with the thermocline generally below $z_{f5} = -2.6$ m significantly reduces $\bar{T}$ at f6 and f7 relative to the shallower f1–f5 (Figures 6a and 6c).

During SC, time-averaged surfzone (f1–f4) $\bar{D}(x,z) < 5$ ppb (Figure 6b), and the variability represents the dye concentration growth early in the release period (Figure 4c). During EQ, dye is approximately stationary at the frames, and $\bar{D}(x,z)$ weakly decreases seaward from f1 to f4 (Figure 6d), consistent with the EQ jetski-measured surface $\bar{D}(x)$ averaged over time and $0 < y < 600$ m (Figure 5b). Farther offshore at f6 and f7, EQ $\bar{D}(x,z)$ decreases significantly (Figure 6d). Although dye spreads offshore and reaches the surface above f6

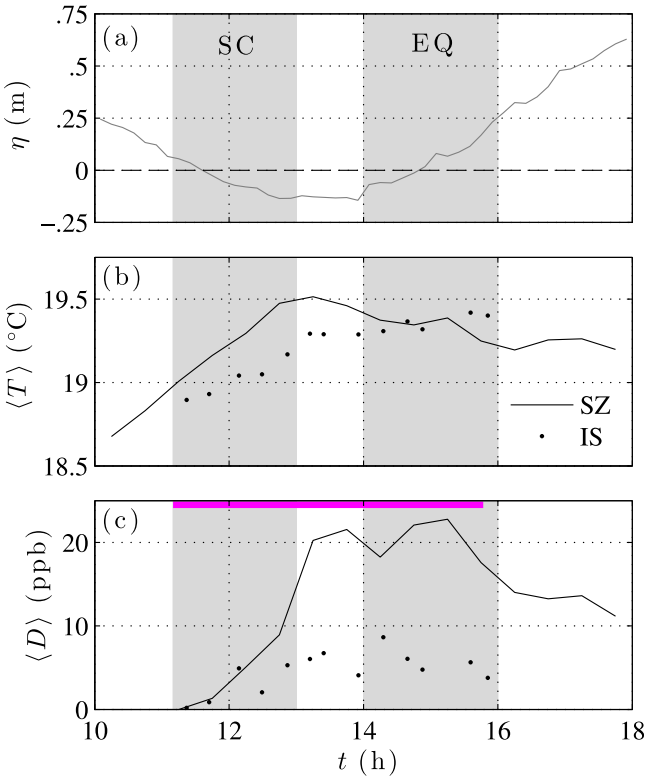

Figure 4. (a) Time-averaged sea level η (measured at f6) relative to mean sea level (dashed), (b) bulk temperature, and (c) bulk dye concentration versus time. In Figures 4b and 4c, surfzone $\langle\,\rangle$ (curves) are cross-shore averages of the surfzone frames f1–f4 ($\bar{z} \approx -1$ m), and inner-shelf $\langle\,\rangle$ (dots) are averages over each alongshore transect at ET1 ($z = -1$ m). Magenta bar in Figure 4c denotes time when dye is released continuously near the shoreline. Gray shaded regions indicate secular change (SC) and equilibration (EQ) time periods.

and f7 (Figure 5b, red, $x_{f6} = -135$ m and $x_{f7} = -199$ m), it does not readily spread vertically down to $(x,z)_{f6} = (-135, -3.6)$ m and $(x,z)_{f7} = (-199, -5.7)$ m (Figure 6d), where the temperature is colder (Figure 6c).

3.4. Vertical Structure of Dye in the Surfzone

The vertical structure of dye concentration is measured at frame f4, located at the approximate seaward surfzone boundary x_b in mean water depth $h_b = 2.1$ m (Figure 3c). Three ETs span 1.1 m vertically (0.2, 0.7, and 1.3 m above the bed). Dye is approximately vertically uniform, indicating that it is well mixed over this water depth (Figure 7). D is very similar at the lower two ETs, while D at the upper ET is sometimes about 1–2 ppb less. The first EOF of dye concentration (not shown) is approximately vertically uniform (11% top-to-bottom variation) and represents 99% of the dye concentration variance.

3.5. Inner-Shelf Alongshore and Vertical Structure of Dye and Temperature

3.5.1. Inner-Shelf Alongshore Transects

A typical inner-shelf alongshore boat transect of dye concentration $D(y,z)$ during SC is alongshore-patchy with approximately 25–50 m wide bands of elevated $D(y,z)$ (Figure 2b), consistent with the aerial photograph of alongshore-patchy dye plumes (Figure 1c). Inner-shelf $T(y,z)$ varies alongshore with structure similar to $D(y,z)$, and the vertical stripes of elevated D and T co-occur (Figures 2b and 2c). Within the dye patches, $D(y,z)$ and $T(y,z)$ are approximately vertically uniform from $z = -1$ to -3 m.

For subsequent analyses of inner-shelf boat transects, the alongshore-towed vertical ET array measurements are decomposed into an along-transect and vertical average and a perturbation, i.e.,

$$T_i(y,z_k) = \langle T\rangle_i + T_i'(y,z_k), \tag{1}$$

where subscript i denotes alongshore transect number (a proxy for the time evolution of T and D) and subscript k denotes the vertical ET location. The mean $\langle T\rangle_i$ is defined as an average over y and z, i.e.,

$$\langle T\rangle_i = \frac{1}{L_{y_i} L_z} \int_{-3\,\mathrm{m}}^{-1\,\mathrm{m}} \int_{y_{i\min}}^{y_{i\max}} T_i(y,z_k)\, dy\, dz, \tag{2}$$

where $L_z = 2$ m is the vertical span of the ET array, and $L_{y_i} = y_{i_{\max}} - y_{i_{\min}}$ is the alongshore span of transect i. D is also decomposed according to equations (1) and (2). $\langle\,\rangle_i$ is similar to the bulk inner-shelf quantity at $z = -1$ m shown in Figures 4b and 4c, but it is also vertically averaged from $z = -1$ to -3 m. This

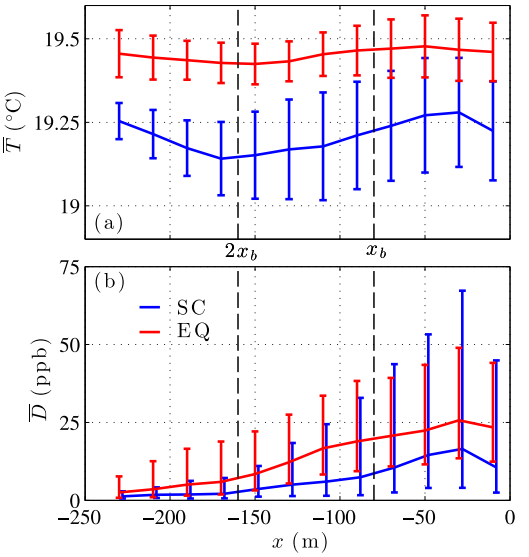

Figure 5. Binned means (time- and alongshore-averaged) of jetski-measured surface (a) temperature and (b) dye concentration versus cross-shore coordinate x during SC (blue) and EQ (red). Vertical bars indicate standard deviations about the means (statistics are computed arithmetically for T and logarithmically for D). Dashed vertical lines indicate the seaward surfzone boundary (x_b) and the mean cross-shore location of inner-shelf alongshore boat transects ($2x_b$).

decomposition separates the T and D variability due to secular changes throughout the day (i.e., temporal variability, $\langle D \rangle_i$) and the variability due to horizontal and vertical structure (i.e., $D_i'(y, z_k)$).

Averaging $T_i'(y, z_k)$ and $D_i'(y, z_k)$ over all alongshore locations and all transects (t = 11:10–16:00 h) gives the ensemble-averaged vertical structures $\overline{T'}(z_k)$ and $\overline{D'}(z_k)$ (Figures 8a and 8b). Consistent with observations from a single inner-shelf alongshore transect (Figure 2b), the mean $\overline{D'}(z_k)$ and standard deviation of $D_i'(y, z_k)$ are approximately vertically uniform (Figure 8b). The vertical variation of ensemble-averaged $\overline{T'}(z_k)$ is weak, and variability of $T_i'(y, z_k)$ is strongest at z = –3 m, where the standard deviation is approximately twice as large as at z = –1 m (Figure 8a). The mean $\overline{D'}(z_k)$ and dye variability computed for SC and EQ separately are similar to those for the 11:10–16:00 h period (Figure 8b). The mean vertical temperature structures $\overline{T'}(z_k)$ during SC and EQ are also similar to the 11:10–16:00 h ensemble average (Figure 8a). However, the standard deviation of $T_i'(y, z_k)$ is approximately twice as large at all z_k during SC as during EQ.

The inner-shelf D_i' and T_i' variability is analyzed with vertical EOFs over 11:10–16:00 h. The first EOF of D_i' (representing 92% of the variance) is approximately vertically uniform (17% top-to-bottom variation), decreasing slightly with depth (Figure 8d). The weak vertical variation of both the mean (Figure 8b) and the first EOF (Figure 8d) indicates that dye is typically well mixed from z = –1 to −3 m, consistent with Figure 2b. The first EOF of T_i' (representing 83% of the variance) increases monotonically with depth, having 72% top-to-bottom variation (Figure 8c). The weak vertical variation of the mean (Figure 8a),

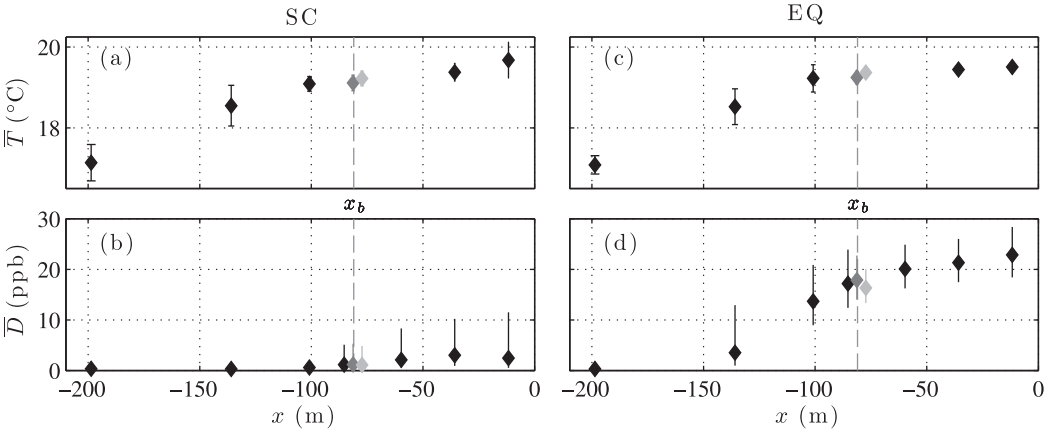

Figure 6. Means (diamonds) and standard deviations (vertical bars) of (top) temperature and (bottom) dye concentration versus cross-shore coordinate x at the cross-shore array (f1-f7, Figure 1b). Left (a and b) and right (c and d) columns are for SC and EQ, respectively. Statistics are computed arithmetically for T and logarithmically for D. Dashed vertical lines are at x_b. Data from f4 are offset laterally for plotting purposes; f4 instruments were located at the same cross-shore coordinate (x_b) 0.2, 0.7, and 1.3 m above the bed (Figure 3c).

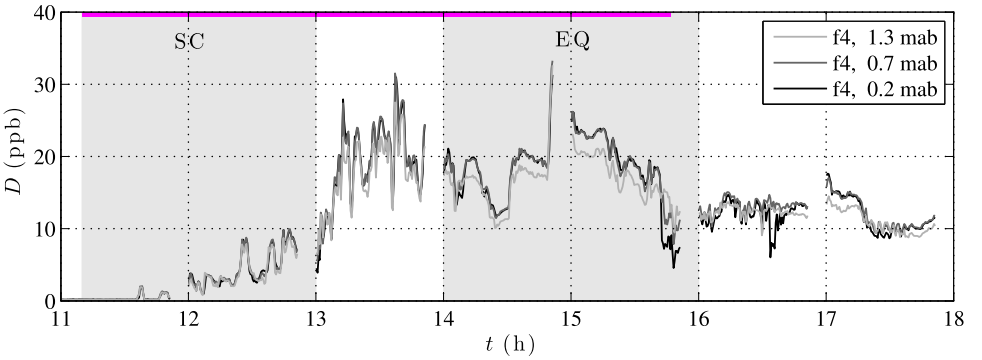

Figure 7. Dye concentration D versus time at the three vertically separated ETs on f4, located 0.2, 0.7, and 1.3 m above the bed (mab) at the seaward surfzone boundary (Figure 3c). Magenta bar shows time when dye is released continuously near the shoreline, 465 m south of the cross-shore array (Figure 1). Shaded regions indicate SC and EQ. Gaps in the time series result from sampling for 51 min of each hour.

combined with the depth-increasing first EOF (Figure 8c), indicates that temperature is often vertically well mixed from $z = -1$ to -3 m (Figure 2c), but that the temperature variability increases from $z = -1$ to -3 m.

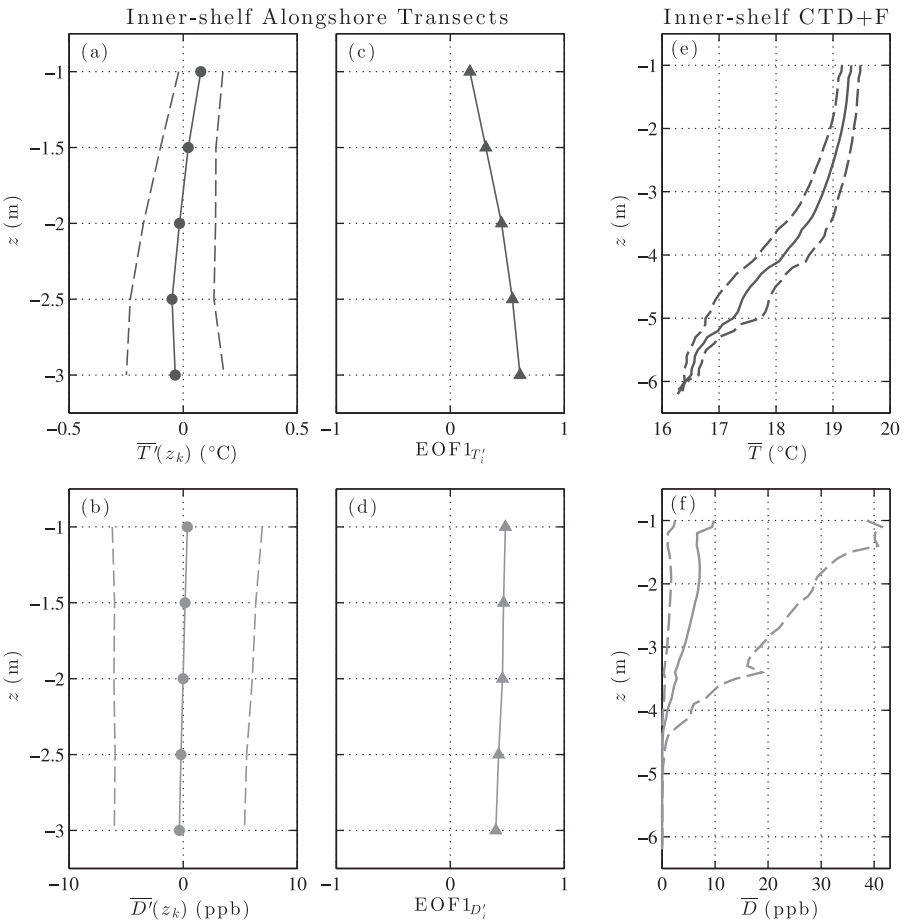

Figure 8. (a and b) Time- (11:10−16:00 h) and alongshore-averages of inner-shelf perturbation temperature $T'_i(y, z_k)$ and dye concentration $D'_i(y, z_k)$ (equations (1) and (2)) versus vertical coordinate z from the alongshore-towed vertical array. Dashed curves indicate standard deviations about the means. (c and d) First EOFs of perturbation T'_i and D'_i versus vertical coordinate z, representing 83% and 92% of the variance, respectively. (e and f) Mean temperature $\bar{T}$ and dye concentration $\bar{D}$ versus vertical coordinate z for 21 dye plume CTD+F casts during 11:49–15:17 h. Dashed curves indicate standard deviations about the means (statistics are computed arithmetically for T and logarithmically for D). Note that the vertical axes of Figures 8e and 8f differ from those of Figures 8a–8d.

3.5.2. CTD+F Casts

Individual CTD+F casts (not shown) within dye plumes in 4–6 m water depth often reveal significant temperature and dye vertical stratification near or below $z \approx -3$ m. Estimated from 21 CTD+F dye plume-contained casts between 11:49 and 15:17 h, mean $\bar{T}(z)$ and $\bar{D}(z)$ vary weakly over the upper 3 m (Figures 8e and 8f), consistent with the inner-shelf alongshore transect $\overline{T'}(z_k)$ and $\overline{D'}(z_k)$ (Figures 8a and 8b). Below $z=-3$ m, $\bar{T}(z)$ decreases rapidly and $\bar{D}(z)$ is near zero. Below $z \approx -4.6$ m, $D \approx 0$ ppb in all casts (Figure 8f), and with the exception of a single cast during SC near the release location ($y = 0$ m), essentially no dye is observed for $T < 18\,^{\circ}$C (Figures 8e and 8f). CTD+F dye variability (dashed, Figure 8f) is largest near the surface, where concentrations are highest. In contrast, T variability is maximum between $z \approx -3$ and -5 m (Figure 8e) owing to variations in thermocline depth.

3.6. Dye-Temperature (D-T) Relationships

The natural temperature tracer has an alongshore-uniform surfzone source during SC (Figures 4b and 5a), which contrasts with the near-shoreline point source (11:10–15:47 h) of anthropogenic dye tracer. Separate analyses of T and D reveal temporal, cross-shore, alongshore, and vertical tracer variability (Figures 2, 4, 5, 6, and 8). To diagnose mechanisms governing D and T transport and mixing, D-T relationships are examined with the inner-shelf alongshore transects and the cross-shore array (Figure 1).

3.6.1. Inner-Shelf Alongshore Transect D-T Relationship

The perturbation dye $D_i'(y, z_k)$ and temperature $T_i'(y, z_k)$ relationship is examined on inner-shelf alongshore transects at the upper-most ($z = -1$ m) and lower-most ($z = -3$ m) vertical locations. During SC, moderately elevated $D_i' > 15$ ppb correspond to warm $T_i' > 0.1\,^{\circ}$C, and the highest $D_i' > 30$ ppb generally correspond to the warmest $T_i' \geq 0.2\,^{\circ}$C at both vertical locations (Figures 9a and 9b). Cold events ($T_i' < -0.25\,^{\circ}$C) correspond to low $D_i' < 10$ ppb, and at $z = -3$ m the coldest water ($T_i' < -0.5\,^{\circ}$C) generally has negative D_i' (Figures 9b and 9d). Although the variability of D_i' and T_i' is reduced during EQ relative to SC (compare right with left columns, Figure 9), the same D_i'-T_i' relationship is observed for both periods: warm water is required for elevated D_i', and cold water has low D_i'.

The highest inner-shelf $D_i' > 30$ ppb, likely surfzone water most recently delivered to the inner-shelf, occur during SC, when the surfzone to inner-shelf temperature difference is largest (Figure 4b). The alongshore structures of inner-shelf D_i' and T_i' are examined at $z = -3$ m for the three SC events when $D_i' > 30$ ppb (Figure 10). During these events, D_i' and T_i' are elevated in approximately 25–50 m wide alongshore bands (Figure 10), and are approximately vertically uniform between $z = -1$ and -3 m (consistent with Figures 8b and 8a). The perturbation temperature T_i' typically varies alongshore by 0.5 °C (Figures 10b1–10b3) and covaries with D_i' (Figures 10a1–10a3), similar to the overall D_i'-T_i' relationship (Figure 9).

Even at alongshore length scales <10 m, D_i' and T_i' are frequently related. For example, during the second event (Figures 10a2 and 10b2), the maximum $D_i' = 38$ ppb at $y - y_{pk} = 0$ m (where y_{pk} is the alongshore location of maximal D_i') corresponds to elevated $T_i' = 0.25\,^{\circ}$C (red symbol in Figures 10a2 and 10b2). At $y - y_{pk} = 9$ m, the local minimum $D_i' = 8$ ppb corresponds to a local minimum $T_i' = -0.15\,^{\circ}$C (green symbol in Figures 10a2 and 10b2). At $y - y_{pk} = 17$ m, secondary maxima of $D_i' = 18$ ppb and $T_i' = 0\,^{\circ}$C coincide (yellow symbol in Figures 10a2 and 10b2). Local D_i' and T_i' minima also coincide another 15 m alongshore at $y - y_{pk} = 32$ m (blue symbol in Figures 10a2 and 10b2). Similar spatial covariability of D_i' and T_i' occurs in the other examples. However, as in Figure 9, this alongshore covariation is not linear since temperature has an alongshore-uniform surfzone source whereas dye has a surfzone point source and decays in the alongshore direction. The alongshore-patchiness (Figures 2 and 10) and general D_i'-T_i' relationship (Figure 9) suggest that inner-shelf lateral mixing is relatively weak.

3.6.2. Cross-Shore Array D-T Relationships

Here the variability and covariability of D and T are examined at the cross-shore array (Figure 1b) over a 13 h period from the start of the dye release (11:10 h). Prior to 18:00 h (including both SC and EQ), the surfzone (f2) is warm with relatively small T variability (Figure 11a, red). On the inner-shelf (f5–f7), mean T decreases and variability increases with distance offshore and depth, with T varying by approximately 1.5 °C and 2 °C at f6 and f7, respectively (Figure 11a). The 18 °C isotherm can migrate as much as 3.1 m vertically in approximately 1.25 h (e.g., $T = 18\,^{\circ}$C at f5 ($z = -2.6$ m) at $t \approx 15{:}45$ h, and $T = 18\,^{\circ}$C at f7 ($z = -5.7$ m) at $t \approx 17{:}00$ h, Figure 11a). At f2, $D > 10$ ppb arrives at $t \approx 12{:}00$ h, about an hour after the release begins (Figure 11b, red). At inner-shelf f5 and f6, significant dye arrives at approximately 12:45 h and 13:30 h,

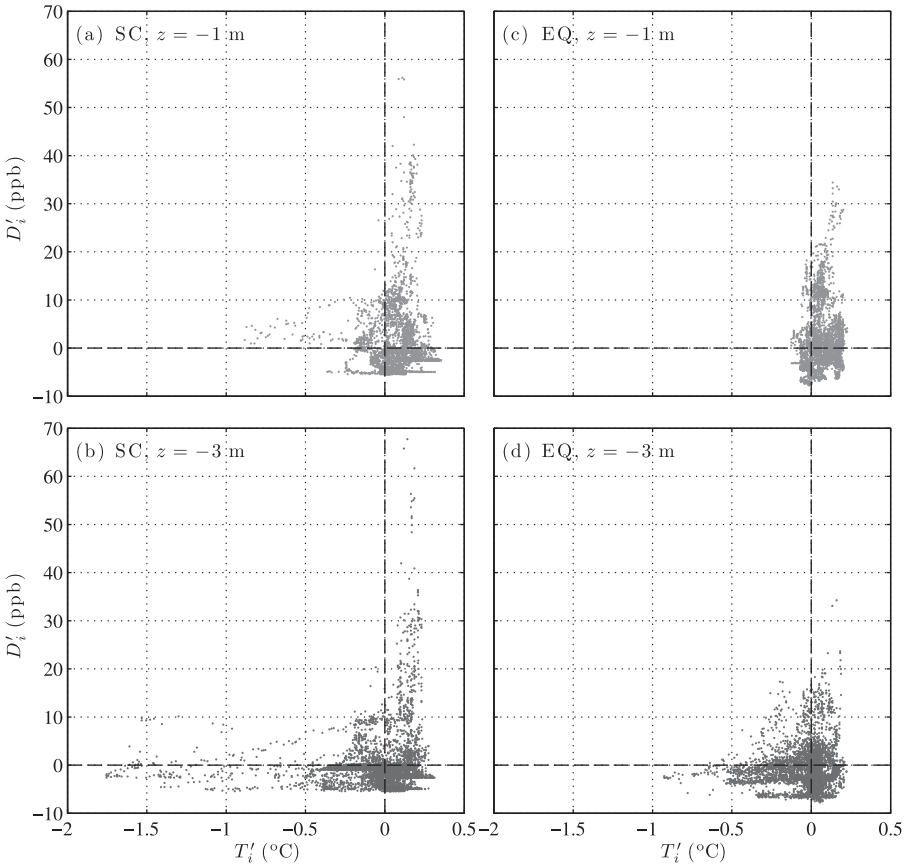

Figure 9. Perturbation dye concentration D_i' versus perturbation temperature T_i' (equations (1) and (2)) for inner-shelf alongshore transects during (a and b) SC and (c and d) EQ at (a and c) $z = -1$ m (ET1) and (b and d) $z = -3$ m (ET5).

respectively (Figure 11b, green and gray). Mean dye concentrations decrease with distance offshore and depth, with comparable D variability among f2, f5, and f6 (Figure 11b).

Mean dye concentrations at f2–f6 begin to decrease at approximately 16:00 h (the continuous dye release stops at 15:47 h, Figure 11b). Prior to 17:00 h, the temperature at f7 is cold (usually <18 °C), and no f7 dye is observed. However, at approximately 17:00 h, f7 T increases above 18 °C (Figure 11a, blue), coinciding with a nonzero D burst at f7 (Figure 11b, blue). Similarly, when f6 $T < 18$ °C, f6 D also becomes negligible (Figures 11a and 11b, gray, $t \approx 15{:}00$ and 16:00 h). Observations at f7 end at 17:30 h.

After 18:00 h, temperature and dye conditions change substantially. T at f2, f5, and f6 is warm (>19 °C) and uniform during 18:00-22:00 h (Figure 11a), indicating a thermocline deepening. Similarly, dye at f2, f5, and f6 is well mixed, particularly from 20:00 to 22:00 h (Figure 11b). Shortly after 22:00 h, thermal stratification reappears, influencing the dye field. For example, as f6 T becomes <18 °C at $t \approx 22{:}30$ h, dye concentration becomes negligible, similar to earlier times when $T < 18$ °C at both f6 and f7 (Figures 11a and 11b). This lack of dye for water colder than 18 °C is consistent with CTD+F vertical profiles. With the exception of a single cast during SC near the release location ($y = 0$ m), no dye is observed for $T < 18$ °C (Figures 8e and 8f).

D-T relationships vary with frame location (Figure 12). During the stationary EQ period, within the surfzone at f2 ($z = -0.4$ m), T variation is small, dye concentration is always relatively high ($D > 15$ ppb), and no clear D-T relationship is evident (Figure 12, red). In contrast, on the inner-shelf at f6 ($z = -3.6$ m), D and T are related linearly for $18 \leq T \leq 19.2$ °C, while for $T < 18$ °C, $D \approx 0$ ppb (Figure 12, gray). Slightly farther onshore at f5 ($z = -2.6$ m, just seaward of the f4 surfzone boundary), the D-T relationship is a blend of that observed at inner-shelf f6 and surfzone f2 (Figure 12, green). At the deepest frame f7 ($z = -5.7$ m), the water is cold ($T < 18$ °C) during EQ, and $D = 0$ ppb throughout this period (Figure 12, blue).

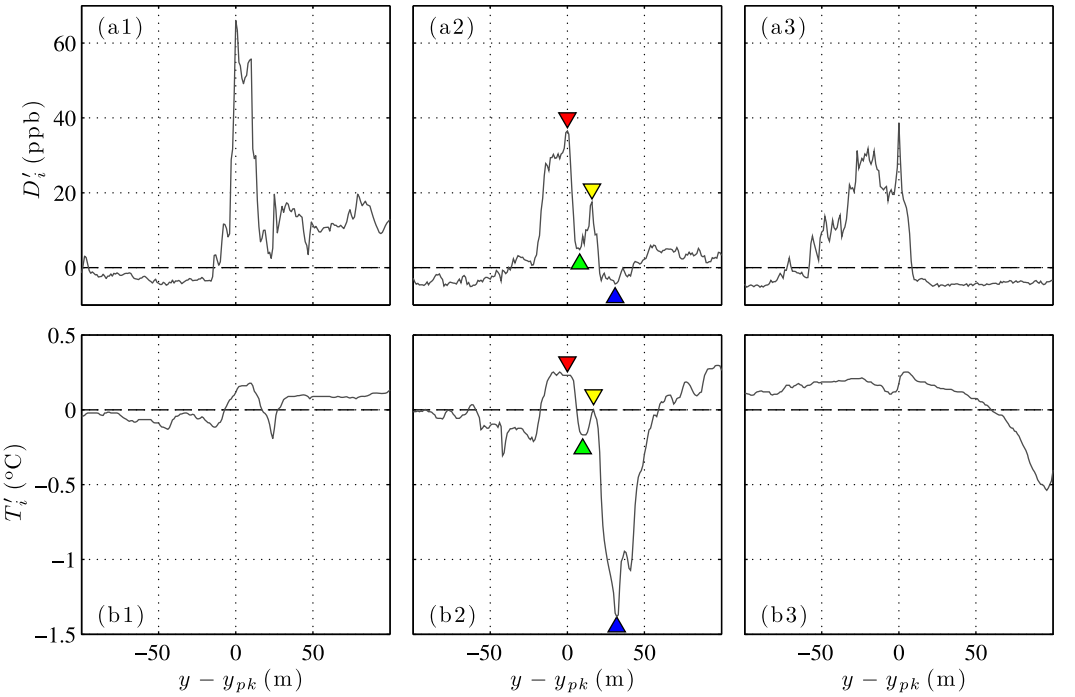

Figure 10. Perturbation (a1–a3) dye concentration D_i' and (b1–b3) temperature T_i' (equations (1) and (2)) at $z=-3$ m (ET5) versus relative alongshore position $y-y_{pk}$ for three case examples (ab1–ab3) where $D_i' > 30$ ppb during SC. For each case, y_{pk} is the alongshore location of maximal D_i', and an alongshore region ± 100 m of y_{pk} is shown. Colored triangles in Figures 10a2 and 10b2 indicate corresponding extrema.

3.7. Surfzone and Inner-Shelf Alongshore Dye Dilution

During EQ, the mean (time- and alongshore-averaged) cross-shore jetski profiles of surface dye show that $\bar{D}(2x_b) \approx 0.4\bar{D}(x_b)$ (Figure 5b, red). Dye at $2x_b$ is consistently observed to be vertically well mixed down to $z = -3$ m (Figure 8b). The inner-shelf ($2x_b$) alongshore-patchiness and *D-T* relationship suggest that horizontal mixing on the inner-shelf is weak, and that inner-shelf dye is locally (at the same y) advected from the surfzone. Such advection would result in vertical dye spreading seaward of x_b ($h = 2.1$ m) which is accounted for by defining a depth-normalized dye concentration $\hat{D}$, where

$$\hat{D} = \begin{cases} D, & \text{for } x \approx x_b \\ \dfrac{3}{2.1}D, & \text{for } x \approx 2x_b \end{cases}. \tag{3}$$

Applying this normalization (3) to the jetski surface observations results in EQ time- and alongshore-averaged $\bar{\hat{D}}(2x_b) \approx 0.6\bar{\hat{D}}(x_b)$. That this ratio is less than but near unity suggests that the assumption of local cross-shore dye advection from the surfzone to $2x_b$ is reasonable. To explore this concept further, the alongshore dilution of dye is examined both within the surfzone and on the inner-shelf.

Mean cross-shore profiles of surface dye concentration $\bar{D}(x, y_j)$ are calculated by averaging the 11:10–16:00 h jetski-measured D over individual transect realizations at designated alongshore locations y_j (not shown). For $y_j \geq 30$ m, the surface $\bar{D}(x, y_j)$ are approximately cross-shore uniform within the surfzone and decay offshore of x_b, similar to the EQ mean cross-shore dye profile in Figure 5b. However, $\bar{D}(x, y_j)$ decrease in the positive alongshore direction both within the surfzone and on the inner-shelf.

The alongshore dilutions of $\hat{D}$ at x_b and $2x_b$ are compared during 13:00–16:00 h (instead of just EQ, 14:00−16:00 h), in order to increase sample sizes during approximately stationary dye conditions, excluding only SC when temporal changes in dye concentrations are large (Figure 4c). We compute $\hat{D}(x_b, y)$ using the cross-shore jetski transects and $\hat{D}(2x_b, y)$ using ET1 ($z = -1$ m) from the alongshore boat transects. $\hat{D}(x_b, y)$ is averaged over a 20 m cross-shore region ($x_b \pm 10$ m). Boat transects are not perfectly alongshore,

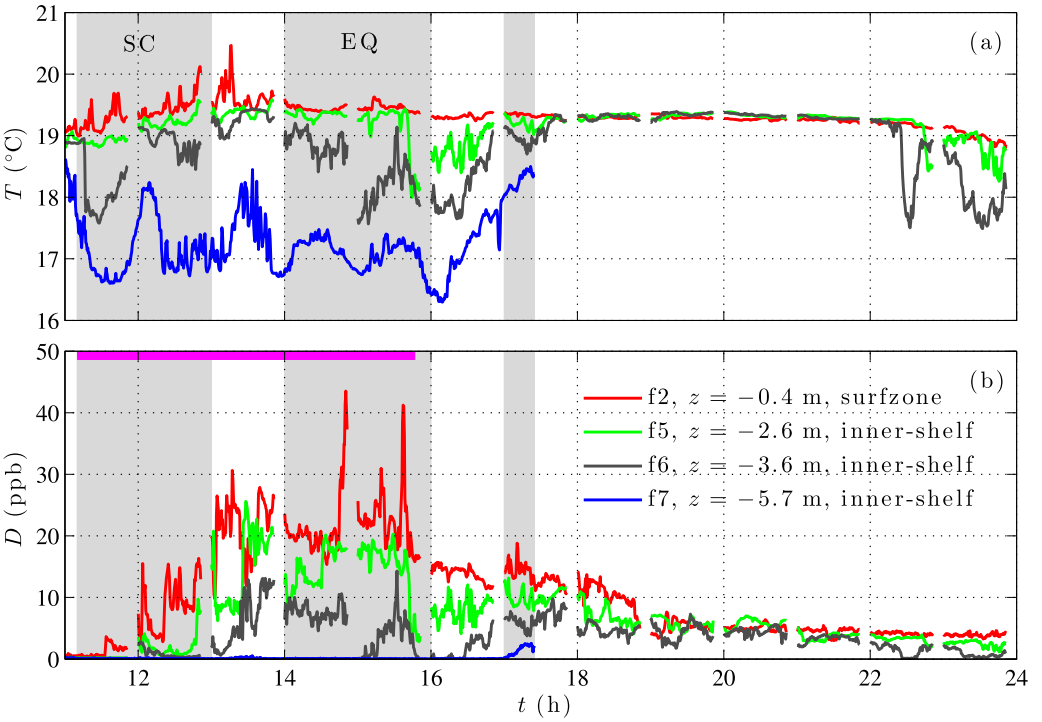

Figure 11. (a) Temperature T and (b) dye concentration D versus time at the cross-shore array within (f2) and seaward of (f5, f6, and f7) the surfzone (see legend and Figure 1b). Magenta bar in Figure 11b denotes time when dye is released near the shoreline, 465 m south of the array (Figure 1, stars). Shaded regions indicate SC and EQ, and a post-EQ period of nonzero D at f7. Note that f7 data are unavailable after t = 17:30 h. Gaps in the f2, f5, and f6 time series result from sampling for 51 min of each hour.

and $\hat{D}(2x_b, y)$ is averaged over an 80 m cross-shore region ($2x_b \pm 40$ m). The data are alongshore-binned using the same bins for $\hat{D}(x_b, y)$ and $\hat{D}(2x_b, y)$, with bin widths ranging from Δy=50 m (nearest the dye release) to $\Delta y = 240$ m (farthest from the release).

Alongshore dilutions of $\hat{D}(x_b, y)$ and $\hat{D}(2x_b, y)$ are similar (Figure 13) and consistent with a power-law in y, i.e.,

$$\hat{D} = \hat{D}_0 (y/y_0)^{\alpha}, \tag{4}$$

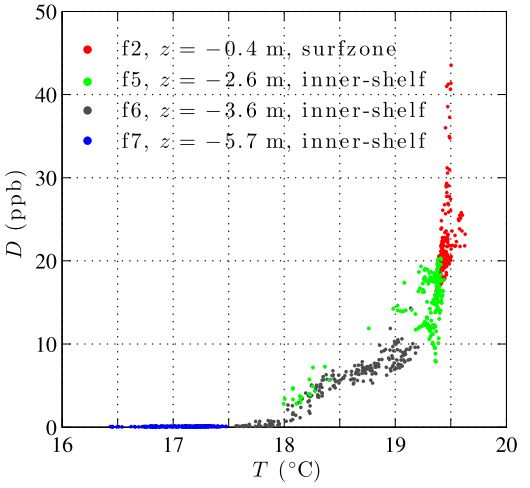

Figure 12. Dye concentration D versus temperature T at cross-shore array instruments within (f2) and seaward of (f5, f6, and f7) the surfzone during EQ.

where $\hat{D} = \hat{D}_0$ at $y = y_0$, and $y_0 = 1$ m is chosen for simplicity. The best fit $\hat{D}_0$ at x_b and $2x_b$ are 42 and 30 ppb, respectively, and best fit power-law exponents at x_b and $2x_b$ are $\alpha = -0.19$ and -0.21, respectively (dashed lines in Figure 13). The ratio $\hat{D}_0(2x_b)/\hat{D}_0(x_b) \approx 0.7$, consistent with alongshore-averaged $\bar{\hat{D}}(2x_b)/\bar{\hat{D}}(x_b) \approx 0.6$. The downstream dye dilutions can also be fit with exponentials, resulting in alongshore decay scales $L_{\text{eff}} \approx 1350$ m, that give approximately linear decay for the observed alongshore region ($y < 700$ m). For $y > 75$ m, the best fit exponentials have similar but slightly larger root-mean-square (rms) errors than the best fit power-laws (4). However, for $y < 75$ m, the exponential fits significantly under-predict the observed dye concentrations. The dye dilution rates farther downstream ($y > 700$ m) are unknown.

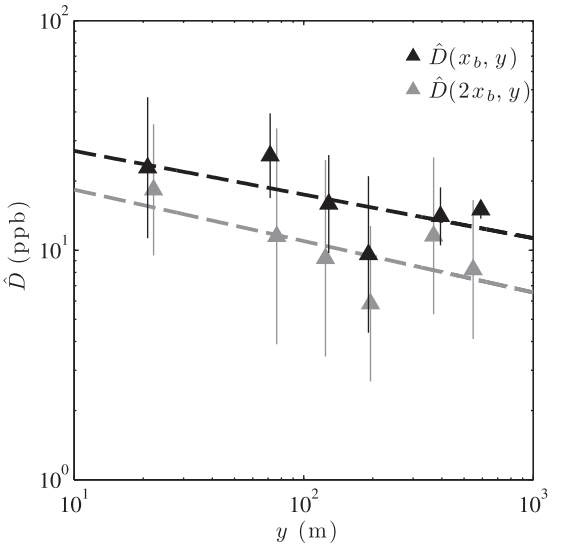

Figure 13. Alongshore-binned means (13:00–16:00 h, symbols) and standard deviations (vertical bars, statistics computed logarithmically) of depth-normalized dye concentration $\hat{D}$ (equation (3)) versus alongshore distance y from dye release ($y = 0$ m) observed at the seaward surfzone boundary x_b (black) and the inner-shelf $2x_b$ (gray). Best fit slopes (dashed) are -0.19 and -0.21, respectively.

The similar downstream dye dilutions for both the surfzone and inner-shelf, together with the inner-shelf alongshore-patchiness and *D-T* relationship, indicate that inner-shelf dye is locally (at the same y) cross-shore advected from the surfzone. The downstream dilution power-law exponents $\alpha \approx -0.2$ are smaller than those observed and modeled for surfzone-contained dye plumes ($\alpha \approx -0.5$ [*Clark et al*., 2010]), indicating that once the surfzone is saturated with dye, the dilution rate slows. As the surfzone-contained plume model [*Clark et al*., 2010] uses a constant cross-shore surfzone diffusivity, the difference between the IB09 and surfzone-contained power-law exponents further indicates that cross-shore diffusivity on the inner-shelf is reduced relative to the surfzone.

3.8. Alongshore Dye Transport

The alongshore dye transport observed during 11:10–24:00 h at the cross-shore array 465 m downstream from the release location (Figure 1a) is compared with the near-shoreline dye release rate ($Q_R = 717.45$ ppb m^3 s^{-1} during 11:10–15:47 h, total release amount $\mathcal{V}_R = 1.19\times10^7$ ppb m^3). Dye is advected from the release location $(x, y) = (-10, 0)$ m toward the cross-shore array by the northward ($+y$) alongshore current V. Assuming vertically uniform $V(x,t)$ and $D(x,t)$ in the surfzone (between the shoreline and f4), the surfzone alongshore dye transport M^y_{SZ} is

$$M^y_{SZ}(t) = \int_{x_b}^{0} d(x,t)V(x,t)D(x,t)\,dx, \tag{5}$$

where 30 s averaged total water depth $d = h+\eta$, V, and D are used. $D(x,t)$ generally varies between 0 and 30 ppb (Figures 6b and 6d), and V is usually northward with maximum 0.25 m s^{-1} (Figure 3b). The surfzone alongshore dye transport M^y_{SZ} becomes significant around 13:00 h and generally varies between approximately 0 and 450 ppb m^3 s^{-1}, fluctuating at infragravity and very low frequency (VLF) time scales (Figure 14a). By 24:00 h, M^y_{SZ} decreases to ≈ 40 ppb m^3 s^{-1} (when, e.g., f2 $D \approx 4$ ppb, Figure 11b, red). The 11:10–24:00 h time-averaged $\bar{M}^y_{SZ} = 124$ ppb m^3 s^{-1}, and the 13:00–16:00 h average $\bar{M}^y_{SZ} = 208$ ppb m^3 s^{-1} (Figure 14a), about 17% and 29% of the dye injection rate Q_R, respectively.

The ratio of the cumulative (time-integrated) surfzone alongshore dye transport to the total amount of dye released is

$$\Gamma^y_{SZ}(t) = \frac{\int_{t_0}^{t} M^y_{SZ}(\tau)\,d\tau}{\mathcal{V}_R}, \tag{6}$$

where $t_0 = 11{:}10$ h is the dye release start time. Γ^y_{SZ} increases approximately linearly between 13:00 and 18:30 h, increases more slowly until 22:30 h, and roughly equilibrates thereafter (Figure 14b). About 20% of the total dye released is surfzone alongshore transported through the cross-shore array ($y_f = 465$ m) between 13:00 and 16:00 h (dye released 11:10–15:47 h at $y = 0$ m), and another $\approx 25\%$ of the total between 16:00 and 24:00 h. At $t = 24{:}00$ h, approximately 8 h after the end of the dye release, 46% of the released dye has been alongshore transported through the surfzone portion of the cross-shore array (Figure 14b). Seaward cross-shore dye fluxes across the surfzone boundary are discussed in section 4.3.1.

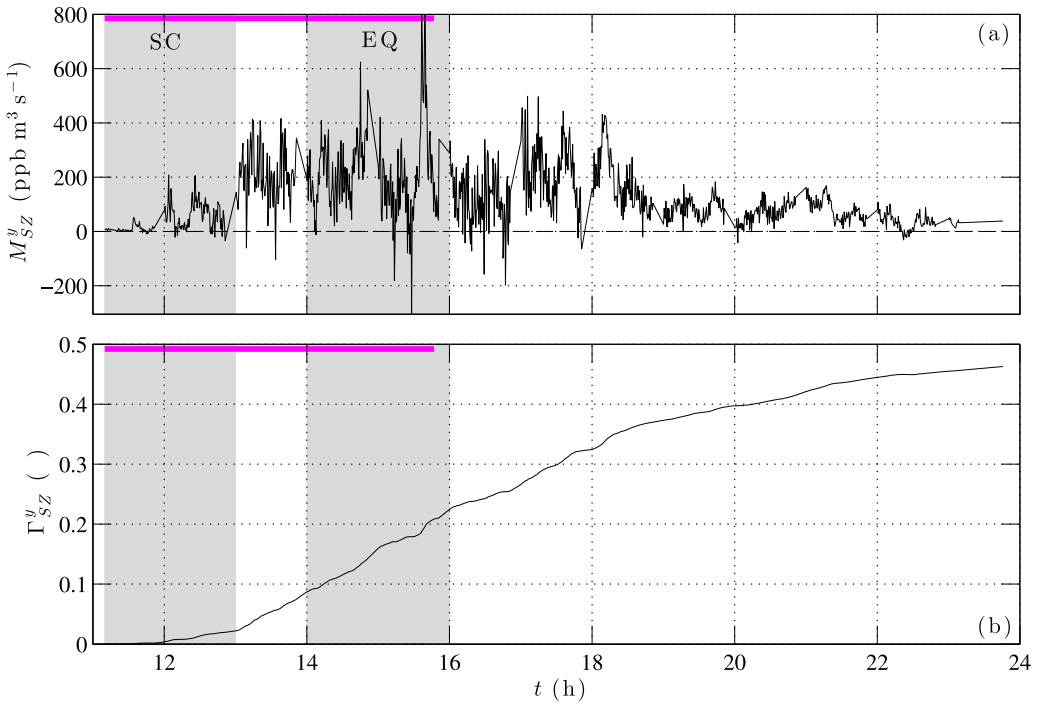

Figure 14. (a) Surfzone (x=0 m to x_b=−81 m) alongshore dye transport at the cross-shore array (465 m north of dye release) versus time. Positive transport is northward. Shaded regions denote periods SC and EQ. Magenta bar denotes dye release period. (b) Cumulative (time-integrated) surfzone alongshore dye transport relative to the total amount of released dye (Γ^y_{SZ} is defined in (6)) versus time.

4. Discussion

4.1. Inner-Shelf Vertical Dye Mixing: Vertical D and T Gradients

Within the surfzone, dye is vertically well mixed (Figure 7). On the inner-shelf, D is largely vertically uniform from z = –1 to −3 m (Figure 8b). At f6 and f7, both located below z = –3 m, nonzero D is only observed for $T \geq 18$ °C (Figure 11), even out to t = 24:00 h, 13 h after the dye release begins. From CTD+F casts (Figures 8e and 8f), dye concentrations decrease below z = –3 m, nonzero D (>1 ppb) is not observed below $z \approx -4.6$ m, and with the exception of a single cast during SC near the release, no dye is observed for $T < 18$ °C. These observations indicate that as dye moves offshore from the well-mixed surfzone, the presence of inner-shelf thermal stratification slows vertical dye mixing.

The effect of temperature stratification on inner-shelf vertical dye mixing is quantified during EQ using vertical D and T gradients estimated between f5 and f6 (Δz=1 m). Their small cross-shore separation Δx=35 m is neglected. During EQ, the observed f5–f6 thermal stratification is variable and sometimes strong, with $\Delta T/\Delta z \approx 0-1.5$ °C m^{-1} (Figure 15), corresponding to Brunt-Väisälä frequencies $N \approx 0-0.05$ Hz. When the thermal stratification is strong (weak), the dye gradients are large (small), and f5–f6 $\Delta D/\Delta z$ and $\Delta T/\Delta z$ are approximately linearly related with a best fit slope 9.7 ppb °C^{-1} (Figure 15). For the same f5–f6 depth range (z = –2.6 to −3.6 m), the CTD+F cast-estimated $\partial D/\partial z$ and $\partial T/\partial z$ (not shown) are similar to the f5–f6 gradients. These observations indicate that thermal stratification can inhibit vertical dye mixing immediately offshore of the turbulent and vertically well-mixed surfzone (f5 and f6 are 19 and 54 m from x_b, respectively, Figure 1).

The effect of temperature stratification on inner-shelf vertical dye mixing is further examined with a dye diffusion model in isotherm coordinates,

$$\frac{\partial D}{\partial t} = \kappa_{TT} \frac{\partial^2 D}{\partial T^2}, \tag{7}$$

where κ_{TT} is the isotherm diffusivity. As surfzone and inner-shelf surface dye concentrations have similar alongshore dilution rates (Figure 13) and inner-shelf alongshore currents are weak (Figure 3b), a local

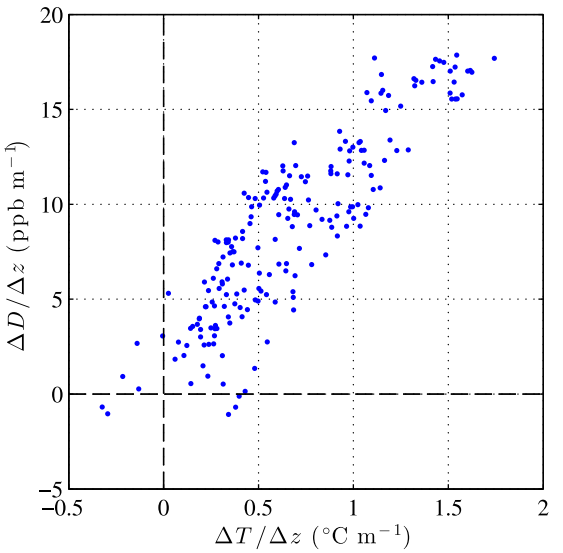

Figure 15. Vertical dye concentration gradient $\Delta D/\Delta z$ versus vertical temperature gradient $\Delta T/\Delta z$ during EQ. Gradients are between inner-shelf frames f5 and f6 ($z=-2.6$ and -3.6 m, respectively). Squared correlation is $r^2=0.79$. Best fit slope is 9.7 ppb °C^{-1}.

(instead of water-following) analysis is acceptable. The temperature domain considered is $T=16-20$ °C. About an hour after arriving at f2, dye arrives at f5 ($\approx$ 13:00 h, Figure 11b) with average f5 concentration $\bar{D} \approx 13$ ppb during EQ (Figure 6d) when the f5 temperature is generally ≥ 19 °C (Figures 6c and 11a). Thus, at $t=$ 13:00 h, a step-function initial condition of $D=13$ ppb for $T \geq 19$ °C and $D=0$ ppb for $T < 19$ °C is used. Boundary conditions $D=13$ ppb at $T=20$ °C and $D=0$ ppb at $T=16$ °C are applied. The top boundary condition simulates a continuous dye source from the warm surfzone.

At 16:00 h, 3 h after dye initially arrives ($T > 18$ °C), observed D is still negligible (<1 ppb) at the 18 °C isotherm (Figure 11). Requiring that after 3 h modeled D at $T=18$ °C is only 5% (0.7 ppb) of the upper layer concentration yields an isotherm diffusivity $\kappa_{TT}=1.5\times10^{-5}$ °C^2 s^{-1}. This estimated κ_{TT} may be biased high, as f6 D is still negligible for $T < 18$ °C even 12 h after the start of the dye release (Figure 11). The modeled D versus T profiles yield a $\partial D/\partial T$ gradient that varies between 7.2 and 9 ppb °C^{-1} during EQ, similar to the f5–f6 observed $(\Delta D/\Delta z)/(\Delta T/\Delta z)=9.7$ ppb °C^{-1} relationship during the same time period (Figure 15). Using the average CTD+F thermal stratification $\partial T/\partial z=0.7$ °C m^{-1} over $z=$ –2.6 to -3.6 m (Figure 8e), the vertical (diapycnal) diffusivity for the f5–f6 depth range is estimated as $\kappa_{zz}=\kappa_{TT}(\partial T/\partial z)^{-2} \approx 3\times10^{-5}$ m^2 s^{-1}, which may also be biased high.

This inferred vertical diffusivity κ_{zz} is only slightly larger than vertical diffusivities 10^{-5} m^2 s^{-1} estimated from observations of dye and microstructure in the largely quiescent ocean interior away from ridges [e.g., *Ledwell et al*., 1993; *Polzin et al*., 1997; *Ledwell et al*., 2011]. The vertical isotherm displacements (Figure 11a), significant inner-shelf stratification (Figure 15), and shallow water depths (Figure 3c) suggest that the 29 September κ_{zz} might be elevated by breaking internal waves (IW). However, the inferred κ_{zz} is quite weak, similar to midcolumn diffusivities of $(0.5-2)\times10^{-5}$ m^2 s^{-1} observed on the summer stratified New England outer-shelf in 70 m water depth during low IW activity [*MacKinnon and Gregg*, 2003]. During spring restratification at the same New England outer-shelf site, average vertical diffusivities during moderate IW (3×10^{-4} m^2 s^{-1}) and strong IW (2×10^{-3} m^2 s^{-1}) events [*MacKinnon and Gregg*, 2005] were 1–2 orders of magnitude larger than the IB09 vertical diffusivity inferred here. Closer to shore (15 m water depth in the Southern California Bight), *Omand et al*. [2012] used observations of vertical nitrate fluxes to estimate bottom boundary layer driven and IW driven diffusivities up to 4×10^{-4} m^2 s^{-1}. Further, the inferred IB09 inner-shelf diffusivity (3×10^{-5} m^2 s^{-1}) is several orders of magnitude smaller than the expected surfzone diffusivities of $10^{-2}-10^{-1}$ m^2 s^{-1} [*Feddersen and Trowbridge*, 2005; *Feddersen*, 2012b]. For the 29 September observations, immediately seaward of the vertically well-mixed surfzone, thermal stratification inhibits vertical mixing between upper layer surfzone influenced water and cooler water below to the magnitude that occurs in ocean interiors.

4.2. Cross-Shore Exchange Velocity

The observations analyzed in sections 3.6.1 and 3.7 indicate that rip currents advect warm, dye-rich surfzone water onto the inner-shelf. Here observations and a two-box temperature model are used to estimate an effective cross-shore exchange velocity u^* between the surfzone and inner-shelf to determine the importance of the transient rip ejections relative to Stokes drift driven advection. The model domain is two-dimensional (assumes alongshore uniformity) and has piecewise linear bathymetry (a triangular surfzone and a trapezoidal inner-shelf). The model has separate surfzone and inner-shelf regions with their own temperatures, and a cross-shore heat flux between the two. Solar radiation heats both regions. No heat flux across the seaward inner-shelf boundary, no heat exchange with the seabed, and no air-sea heat fluxes

(winds were weak) are assumed. The coupled model equations are (subscripts $_{SZ}$ and $_{IS}$ denote surfzone and inner-shelf quantities, respectively)

$$\frac{1}{2}h_{SZ}|x_{SZ}|\frac{dT_{SZ}}{dt}=|x_{SZ}|\frac{R(t)}{\rho c_p}-h_{SZ}u^*(T_{SZ}(t)-T_{IS}(t)), \tag{8a}$$

$$\frac{1}{2}(h_{IS}+h_{SZ})|x_{IS}-x_{SZ}|\frac{dT_{IS}}{dt}=|x_{IS}-x_{SZ}|\frac{R(t)}{\rho c_p}+h_{SZ}u^*(T_{SZ}(t)-T_{IS}(t)), \tag{8b}$$

where $T_{SZ}(t)$ and $T_{IS}(t)$ are the spatially averaged surfzone and inner-shelf temperatures, x_{SZ} and x_{IS} are the seaward boundaries of the surfzone and inner-shelf (with $x = 0$ m at the mean shoreline), h_{SZ} and h_{IS} are the water depths at x_{SZ} and x_{IS}, $\rho=1025$ kg m^{-3} and $c_p=4.0\times10^3$ J kg^{-1} °C^{-1} are the seawater density and specific heat, and $R(t)$ is the incident solar radiation. The depth-integrated temperature flux between the surfzone and inner-shelf is parameterized as $h_{SZ}u^*(T_{SZ}-T_{IS})$, where u^* is an effective cross-shore exchange velocity across the surfzone/inner-shelf boundary $x = x_{SZ}$.

The total incident solar radiation $R(t)$ is inferred from observations of photosynthetically active radiation (PAR, 400–700 nm) measured above the ocean surface at the experiment site (an empirical scaling factor is used to convert from PAR to total solar radiation). Under clear skies, $R(t)$ is approximately constant (at ≈ 575 W m^{-2}) from 10:30 to 13:15 h, after which heavy fog moves in and decreases $R(t)$ by approximately 75%. Choosing $x_{SZ} = x_b$ and $x_{IS} = 2x_b$ (recall $2x_b$ is the mean cross-shore location of inner-shelf alongshore transects) and using observed depths $h_{SZ} = 2.1$ m and $h_{IS} = 4.5$ m, the coupled equations (8a) and (8b) are solved numerically using observations of T_{SZ} and T_{IS} at 10:34 h as initial conditions. Found by minimizing the rms model-data error, the best fit $u^*=8.6\times10^{-3}$ m s^{-1}.

The model solutions agree well with observations, reproducing the differential surfzone and inner-shelf warming prior to 13:15 h and the equilibration of surfzone and inner-shelf temperatures after 13:15 h (Figure 16a, compare symbols and curves). As the surfzone and inner-shelf regions have the same widths, they receive equal cross-shore integrated solar radiation. Yet, because the surfzone is shallower, prior to 13:15 h the solar radiation (magenta curves in Figures 16b and 16c) warms the model surfzone faster than the model inner-shelf (Figure 16a, compare red and blue slopes), consistent with the observations. Both before and after 13:15 h, the cross-shore heat flux has the effect of cooling the warmer surfzone and warming the cooler inner-shelf (cyan curves in Figures 16b and 16c). When fog decreases incident solar radiation at 13:15 h, the cross-shore heat flux becomes the dominant forcing mechanism for both regions (Figures 16b and 16c), resulting in surfzone and inner-shelf equilibration (Figure 16a).

The inferred cross-shore exchange velocity $u^*=8.6\times10^{-3}$ m s^{-1} incorporates all potential surfzone/inner-shelf exchange mechanisms, including both rip currents and Stokes drift driven exchange (onshore near-surface mass flux balanced by undertow at depth). *Clark et al.* [2010] found the Stokes drift driven exchange mechanism to be negligible in surfzone cross-shore dye dispersion due to the surfzone being vertically well mixed (assumed in *Clark et al.* [2010], demonstrated here in Figure 7). However, seaward of the surfzone, where dye concentration is not vertically uniform throughout the water column, Stokes drift driven advection could potentially be an important cross-shore exchange mechanism. Here the magnitude of u^* is compared to that expected for Stokes drift driven exchange offshore of the surfzone.

For normally incident, narrow-banded, slowly shoaling waves, the Stokes drift velocity u_S is shoreward at all depths, and maximum at the surface:

$$u_S=\frac{1}{2}(ak)^2C\frac{\cosh(2k(z+h))}{\sinh^2(kh)}, \tag{9}$$

where a is the wave amplitude, k is the wave number, C is the phase speed, and h is the still water depth. As the IB09 bathymetry and wavefield are approximately alongshore-uniform, the Stokes drift driven exchange is expected to also be alongshore-uniform, with shoreward Stokes drift balanced by a seaward Eulerian return flow u_E such that

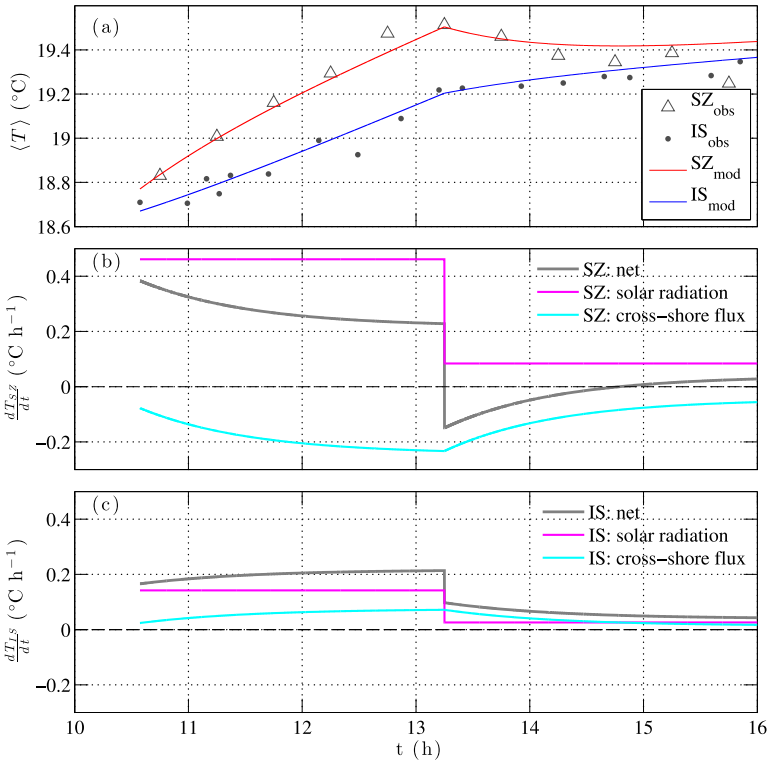

Figure 16. (a) Observed (symbols) and modeled (curves) surfzone and inner-shelf temperature (see legend) versus time. Surfzone $\langle T \rangle$ is 30 min averaged among surfzone-contained frames. Inner-shelf $\langle T \rangle$ is defined in equation (2). Modeled (b) surfzone and (c) inner-shelf temperature time-derivative (gray) versus time, with the contributions from solar heating (magenta) and cross-shore surfzone/inner-shelf heat flux (cyan). Starting at 13:15 h, fog significantly reduces the observed and modeled incident solar radiation.

$$\int_{-h}^{0} u_S \, dz = -\int_{-h}^{0} u_E \, dz. \tag{10}$$

Within the surfzone, the Eulerian flow u_E has been modeled and observed to have a seaward maximum at depth [e.g., *Faria et al*., 2000; *Reniers et al*., 2004]. If a depth-intensified flow were to continue offshore of the surfzone, the seaward of surfzone dye would have a maximum at depth. However, the 29 September seaward of surfzone dye observations show that D is approximately vertically uniform in the upper 3 m, and decreases significantly below 3 m (Figures 8b and 8f). Also, just offshore of the surfzone, u_E profiles have been previously modeled and observed to be largely depth-uniform [*Putrevu and Svendsen*, 1993; *Faria et al*., 2000; *Reniers et al*., 2004; *Kumar et al*., 2012]. Therefore, the seaward of surfzone cross-shore Eulerian flow u_E is assumed vertically uniform,

$$u_E = -\frac{1}{h}\int_{-h}^{0} u_S \, dz = -\frac{1}{2}(ak)^2 \frac{C}{2kh}\frac{\sinh(2kh)}{\sinh^2(kh)}, \tag{11}$$

resulting in net cross-shore Lagrangian flow

$$u_L = u_S + u_E = \frac{1}{2}(ak)^2 \frac{C}{\sinh^2(kh)}\left[\cosh(2k(z+h)) - \frac{\sinh(2kh)}{2kh}\right], \tag{12}$$

which is shoreward near the surface and seaward at depth.

The observed waves are assumed normally incident and narrow banded so $a = H_s/(2\sqrt{2})$. At f5 ($x = -100$ m, the seaward of surfzone frame closest to the surfzone boundary $x_b = -81$ m), the 11:00–16:00 h average incident wave height $H_s = 0.66$ m, peak period $T_p = 14$ s, and water depth $h = 2.9$ m. From (12), u_L at f5 is

shoreward in the upper water column and seaward only below $z=-1.24$ m. Averaging vertically over the seaward portion of the velocity profile yields $\bar{u}_{L_{sea}}=8.7\times10^{-4}$ m s^{-1}, an order of magnitude smaller than the inferred seaward exchange velocity $u^*=8.6\times10^{-3}$ m s^{-1}. Similarly at f6 ($x=-135$ m), $\bar{u}_{L_{sea}}=5.8\times10^{-4}$ m s^{-1}, and u_L is seaward only below $z=-1.78$ m. Inner-shelf observations at $x\approx 2x_b$ (offshore of f6) show that dye (which has a vertically mixed surfzone source) is approximately vertically uniform above $z=-3$ m (Figure 8b). This requires seaward dye advection in the upper water column, which is inconsistent with the Stokes drift driven exchange mechanism (shoreward in the upper water column and seaward at depth). Furthermore, inner-shelf D and T are distinctively alongshore-patchy (Figures 2 and 10), but the Stokes drift driven exchange is expected to be approximately alongshore-uniform. These discrepancies in magnitude, vertical structure, and alongshore-patchiness suggest that the observed surfzone/inner-shelf cross-shore tracer exchange is dominated by transient rip ejections on this day with moderate waves. Stokes drift driven exchange may be important farther seaward of $2x_b$ [*Lentz et al.*, 2008]. Future analyses of dye releases on days with varying waves, tides, winds, and stratification may reveal the effects of these conditions on cross-shore tracer exchange between the surfzone and inner-shelf.

Here the inferred surfzone/inner-shelf cross-shore heat flux is compared to other cross-shelf heat flux estimates during similar times of the year (late summer and early fall). During SC, when a surfzone/inner-shelf temperature difference is consistently present, the depth-normalized cross-shore heat flux across the surfzone/inner-shelf boundary ($h_b=2.1$ m) is $\rho c_p u^* \Delta T \approx 10$ kW m^{-2} in the seaward direction. Farther offshore in 20 m water depth near Mission Beach, California (≈ 30 km north of the IB09 experiment site), *Lucas et al.* [2011] observed a depth-normalized cross-shelf heat flux of ≈ 7 kW m^{-2} that was shoreward, dominated by the semidiurnal internal tide. *Fewings and Lentz* [2011] observed the mean upwelling circulation in 12 m water depth in the Middle Atlantic Bight, where they measured a seaward cross-shelf heat flux of ≈ 15 kW m^{-2}, and concluded that the mean upwelling circulation was likely driven by a combination of surface gravity waves [*Lentz et al.*, 2008], tidal rectification [*Fewings et al.*, 2008], and an alongshelf pressure gradient [*Lentz*, 2008]. These 29 September IB09 observations suggest that transient rip ejections can drive cross-shore surfzone/inner-shelf heat fluxes with depth-normalized magnitudes comparable to those of much larger-scale shelf processes.

4.3. Surfzone Tracer Transports and Downstream Dilution

4.3.1. Cross-Shore Dye Transport

Here the surfzone to inner-shelf cross-shore dye transport is estimated following the two-box model for temperature (8) and is compared to the dye release rate and the alongshore surfzone dye transport (5). The cross-shore dye flux F^x_{SZ} from the surfzone to the inner-shelf is estimated as

$$F^x_{SZ}=h_b u^* \Delta\bar{D}, \tag{13}$$

where h_b is the water depth at the surfzone boundary x_b, u^* is the best fit exchange velocity (section 4.2), and $\Delta\bar{D}=\bar{D}_{SZ}-\bar{D}_{IS}$ is the surfzone and inner-shelf mean dye concentration difference. Using $\bar{D}_{IS}=0.4\bar{D}_{SZ}=0.4D_{0_{SZ}}(y/y_0)^{\alpha}$ (section 3.7) in (13) yields

$$F^x_{SZ}=0.6h_b u^* D_{0_{SZ}}(y/y_0)^{\alpha}, \tag{14}$$

which is valid only during 13:00–16:00 h when the downstream dye dilution has been fit with the power-law (4). The surfzone to inner-shelf cross-shore dye transport between the dye release location ($y=0$ m) and the cross-shore array ($y_f=465$ m) is then

$$M^x_{SZ}=\int_0^{y_f} F^x_{SZ}\,dy=\frac{0.6h_b u^* D_{0_{SZ}}}{\alpha+1}\left(\frac{y_f}{y_0}\right)^{\alpha+1} y_0\,. \tag{15}$$

The best fit $D_{0_{SZ}}=42$ ppb and $\alpha=-0.19$ (section 3.7) yield $M^x_{SZ}=81$ ppb m^3 s^{-1}, about 11% of the instantaneous dye release rate Q_R. The cross-shore dye transport can also be estimated using exponential downstream dilution instead of the power-law (4), with similar results. During 13:00–16:00 h, the cross-shore dye transport M^x_{SZ} between the dye source and y_f is approximately 40% of the mean alongshore

surfzone dye transport $\bar{M}^{y}_{SZ}=208$ ppb m^3 s^{-1} at y_f. Given that nonnegligible alongshore surfzone dye transport M^{y}_{SZ} is observed long after the release ends (Figure 14a), it is likely that M^{x}_{SZ} changes sign (becoming shoreward) as inner-shelf-accumulated dye (which has slow alongshore advection) is recycled back into the surfzone when the last of the surfzone-released dye would have otherwise been alongshore-advected past $y_f=465$ m.

4.3.2. Alongshore Surfzone Dilution Models

Using aerial photographs and in situ measurements, *Inman et al.* [1971] estimated surfzone tracer concentrations to decay exponentially with alongshore distance from the source. Using historical fecal indicator bacteria (FIB) data, *Boehm* [2003] also observed exponential alongshore surfzone decay and developed a differential equation based model, which in steady state, shows agreement with the discretized *Inman et al.* [1971] model. *Grant et al.* [2005] developed both time-varying and steady state solutions for a differential equation model similar to that of *Boehm* [2003]. Based on dye and FIB observations, *Grant et al.* [2005] concluded that, to a good approximation, the steady state model was valid for the moderate environmental conditions during their field observations.

However, a key assumption of *Boehm* [2003] and *Grant et al.* [2005] is that inner-shelf tracer accumulation is negligible, so that no cross-shore tracer recycling from the inner-shelf to the surfzone occurs. This might be a reasonable assumption for FIB when inferred mortality rates are larger seaward of the surfzone [e.g., *Rippy et al.*, 2013]. However, for 29 September IB09 dye tracer, there is significant inner-shelf dye accumulation (Figures 4c, 5b, and 13). Further, the prolonged presence of surfzone dye several hours after the end of the dye release (Figures 11b and 14b) suggests recycling of inner-shelf-accumulated dye back into the surfzone. Thus, in general, inner-shelf tracer accumulation and recycling to the surfzone must be considered for the long-time downstream evolution of surfzone-source tracers.

5. Summary

Cross-shore tracer exchange between the surfzone ($\leq$2 m water depth) and inner-shelf ($\approx 3-6$ m water depth) was examined with 29 September IB09 (Imperial Beach, CA 2009) field experiment observations of temperature and Rhodamine WT dye (released continuously near the shoreline in an alongshore current from 11:10 to 15:47 h). Temperature and dye concentration were measured using a near-bed cross-shore array, repeated cross-shore surface transects at various alongshore locations, inner-shelf CTD+F casts, and a unique, inner-shelf alongshore-towed vertical array.

Prior to 13:00 h, the surfzone and inner-shelf regions both warmed, and the surfzone was consistently warmer than the inner-shelf. Thereafter, heavy fog reduced incident solar radiation significantly, and surfzone and inner-shelf temperatures equilibrated. From 14:00 to 16:00 h, surfzone and inner-shelf temperatures and dye concentrations were roughly stationary. Surfzone dye was laterally and vertically well mixed. Inner-shelf temperature and dye concentration were often alongshore-patchy with coincident warm and dye-rich water. Inner-shelf dye was generally vertically well mixed in a 3 m thick upper layer, but dye concentration decreased below 3 m, where thermal stratification was strong. At the cross-shore array, inner-shelf dye and temperature variability was significant (temperature fluctuations up to 2 °C h^{-1}), dye concentration and temperature were linearly related, and nonzero dye was not observed for water $<$18 °C, even 13 h after the dye release began. The alongshore dilutions of surfzone and inner-shelf dye were similar and followed a power-law relationship with exponents ≈ -0.2, smaller than that previously observed and modeled for surfzone-contained dye plumes (exponent ≈ -0.5). At the cross-shore array, 465 m downstream of the release location, the alongshore dye transport within the surfzone accounted for approximately half of the total dye released.

The vertical mixing of dye below 3 m was inhibited by thermal stratification, where vertical dye and temperature gradients were linearly related. Observations and an isotherm-coordinate dye diffusion model were used to infer a very weak inner-shelf vertical dye diffusivity of $\approx 3\times10^{-5}$ m^2 s^{-1}, suggesting that, immediately offshore of the well-mixed surfzone, thermal stratification can inhibit vertical mixing to levels similar to those observed in ocean interiors. Observations and a model of surfzone and inner-shelf temperature were used to estimate an effective cross-shore surfzone/inner-shelf exchange velocity $u^*=8.6\times10^{-3}$ m s^{-1}.

The inner-shelf dye and temperature alongshore-patchiness and consistent dye-temperature relationship indicate that inner-shelf lateral mixing was relatively weak. Similar surfzone and inner-shelf downstream

dye dilution rates indicate that inner-shelf dye and temperature properties were determined by local cross-shore advection from the surfzone. Together with magnitude and vertical structure discrepancies between u^* and Stokes drift driven velocities, the inner-shelf tracer alongshore-patchiness indicates that transient rip current ejection events were the dominant cross-shore surfzone/inner-shelf exchange mechanism at the alongshore-uniform Imperial Beach on 29 September.

The inferred depth-normalized cross-shore heat flux induced by these transient rip ejections is comparable to IW driven and subtidal circulation driven heat fluxes. During the dye release, the cross-shore surfzone to inner-shelf dye transport between the release point and 465 m downstream, estimated with u^* and power-law alongshore dye dilution, was approximately 40% of the alongshore surfzone dye transport measured 465 m downstream of the release. The significant levels of alongshore surfzone dye transport up to 8 h after the end of the release indicate that dye that accumulated on the inner-shelf (where alongshore advection was slow) was recycled back into the surfzone. This is inconsistent with existing surfzone box models that treat the inner-shelf as a tracer sink.

Acknowledgments

This work comprises the first chapter of Kai Hally-Rosendahl's PhD thesis. As subsequent thesis chapters will use these same IB09 data, they are not shared with this work. However, upon completion of K. Hally-Rosendahl's thesis, IB09 data will be made available at http://falk.ucsd.edu in accordance with the AGU data policy. Kai Hally-Rosendahl was supported by the National Science Foundation Graduate Research Fellowship under grant DGE1144086. IB09 field work and analysis was supported by NSF, ONR, and CA Sea Grant. Staff and students from the Integrative Oceanography Division (B. Woodward, B. Boyd, K. Smith, D. Darnell, R. Grenzeback, A. Gale, M. Spydell, D. Clark, M. Omand, M. Yates, M. Rippy, and A. Doria) were instrumental in acquiring the field observations. K. Millikan, D. Ortiz-Suslow, M. Fehlberg, and E. Drury provided field assistance. Imperial Beach lifeguards, supervised by Captain R. Stabenow, helped maintain safety at this public beach and generally facilitated our work. The YMCA Surf Camp management generously allowed extensive use of their facility for staging and recuperation. The US Navy allowed access to their beach. M. Okihiro coordinated permits and logistics. M. Spydell provided useful feedback. Two anonymous reviewers helped improve this paper. We thank these individuals and organizations.

References

Austin, J. A., and S. J. Lentz (2002), The inner shelf response to wind-driven upwelling and downwelling, *J. Phys. Oceanogr.*, *32*, 2171–2193.

Boehm, A., B. Sanders, and C. Winant (2002), Cross-shelf transport at Huntington Beach. Implications for the fate of sewage discharged through an offshore ocean outfall, *Environ. Sci. Technol.*, *36*(9), 1899–1906, doi:10.1021/es0111986.

Boehm, A. B. (2003), Model of microbial transport and inactivation in the surf zone and application to field measurements of total coliform in northern orange county, California, *Environ. Sci. Technol.*, *37*(24), 5511–5517, doi:10.1021/es034321x.

Clark, D. B., F. Feddersen, M. M. Omand, and R. T. Guza (2009), Measuring fluorescent dye in the bubbly and sediment laden surfzone, *Water Air Soil Pollut.*, *204*, 103–115, doi:10.1007/s11270-009-0030-z.

Clark, D. B., F. Feddersen, and R. T. Guza (2010), Cross-shore surfzone tracer dispersion in an alongshore current, *J. Geophys. Res.*, *115*, C10035, doi:10.1029/2009JC005683.

Clark, D. B., S. Elgar, and B. Raubenheimer (2012), Vorticity generation by short-crested wave breaking, *Geophys. Res. Lett.*, *39*, L24604, doi:10.1028/2012GL054034.

Faria, A. F. G., E. B. Thornton, T. C. Lippmann, and T. P. Stanton (2000), Undertow over a barred beach, *J. Geophys. Res.*, *105*, 16,999–17,010.

Feddersen, F. (2012a), Observations of the surfzone turbulent dissipation rate, *J. Phys. Oceanogr.*, *42*, 386–399, doi:10.1175/JPO-D-11–082.1.

Feddersen, F. (2012b), Scaling surfzone dissipation, *Geophys. Res. Lett.*, *39*, L18613, doi:10.1029/2012GL052970.

Feddersen, F., and J. H. Trowbridge (2005), The effect of wave breaking on surf-zone turbulence and alongshore currents: A modeling study, *J. Phys. Oceanogr.*, *35*, 2187–2204.

Fewings, M., S. J. Lentz, and J. Fredericks (2008), Observations of cross-shelf flow driven by cross-shelf winds on the Inner Continental Shelf, *J. Phys. Oceanogr.*, *38*(11), 2358–2378, doi:10.1175/2008JPO3990.1.

Fewings, M. R., and S. J. Lentz (2011), Summertime cooling of the shallow continental shelf, *J. Geophys. Res.*, *116*, C07015, doi:10.1029/2010JC006744.

Grant, S. B., J. H. Kim, B. H. Jones, S. A. Jenkins, J. Wasyl, and C. Cudaback (2005), Surf zone entrainment, along-shore transport, and human health implications of pollution from tidal outlets, *J. Geophys. Res.*, *110*, C10025, doi:10.1029/2004JC002401.

Haller, M., D. Honegger, and P. Catalan (2014), Rip current observations via marine radar, *J. Waterw. Port Coastal Ocean Eng.*, *140*(2), 115–124, doi:10.1061/(ASCE)WW.1943–5460.0000229.

Harris, T. F. W., J. M. Jordaan, W. R. McMurray, C. J. Verwey, and F. P. Anderson (1963), Mixing in the surf zone, *Int. J. Air Water Pollut.*, *7*, 649–667.

Inman, D. L., R. J. Tait, and C. E. Nordstrom (1971), Mixing in the surf zone, *J. Geophys. Res.*, *26*, 3493–3514.

Johnson, D., and C. Pattiaratchi (2006), Boussinesq modelling of transient rip currents, *Coastal Eng.*, *53*(5), 419–439.

Kirincich, A. R., S. J. Lentz, and J. A. Barth (2009), Wave-driven inner-shelf motions on the Oregon Coast, *J. Phys. Oceanogr.*, *39*(11), 2942–2956, doi:10.1175/2009JPO4041.1.

Koh, R. C. Y., and N. H. Brooks (1975), Fluid mechanics of waste-water disposal in the ocean, *Annu. Rev. Fluid Mech.*, *7*, 187–211, doi:10.1146/annurev.fl.07.010175.001155.

Kumar, N., G. Voulgaris, J. C. Warner, and M. Olabarrieta (2012), Implementation of the vortex force formalism in the coupled ocean-atmosphere-wave-sediment transport (COAWST) modeling system for inner shelf and surf zone applications, *Ocean Modell.*, *47*, 65–95, doi:10.1016/j.ocemod.2012.01.003.

Ledwell, J., A. Watson, and C. Law (1993), Evidence for slow mixing across the pycnocline from an open-ocean tracer-release experiment, *Nature*, *364*(6439), 701–703, doi:10.1038/364701a0.

Ledwell, J. R., L. C. St Laurent, J. B. Girton, and J. M. Toole (2011), Diapycnal mixing in the Antarctic Circumpolar Current, *J. Phys. Oceanogr.*, *41*(1), 241–246, doi:10.1175/2010JPO4557.1.

Lentz, S. J. (2008), Observations and a model of the mean circulation over the Middle Atlantic Bight continental shelf, *J. Phys. Oceanogr.*, *38*(6), 1203–1221, doi:10.1175/2007JPO3768.1.

Lentz, S. J., M. Fewings, P. Howd, J. Fredericks, and K. Hathaway (2008), Observations and a model of undertow over the Inner Continental Shelf, *J. Phys. Oceanogr.*, *38*(11), 2341–2357, doi:10.1175/2008JPO3986.1.

Lucas, A., P. Franks, and C. Dupont (2011), Horizontal internal-tide fluxes support elevated phytoplankton productivity over the inner continental shelf, *Limnol. Oceanogr.: Fluids Environ.*, *1*, 56–74, doi:10.1215/21573698-1258185.

MacKinnon, J. A., and M. C. Gregg (2003), Mixing on the late-summer new england shelf - solibores, shear, and stratification, *J. Phys. Oceanogr.*, *33*(7), 1476–1492, doi:10.1175/1520-0485(2003)033<1476:motlne>2.0.co;2.

MacKinnon, J. A., and M. C. Gregg (2005), Spring mixing: Turbulence and internal waves during restratification on the New England shelf, *J. Phys. Oceanogr.*, *35*(12), 2425–2443, doi:10.1175/jpo2821.1.

MacMahan, J., A. Reniers, E. Thornton, and T. Stanton (2004), Infragravity rip current pulsations, *J. Geophys. Res.*, *109*, C01033, doi:10.1029/2003JC002068.

MacMahan, J., et al. (2010), Mean Lagrangian flow behavior on an open coast rip-channeled beach: A new perspective, *Mar. Geol.*, *268*(14), 1–15, doi:10.1016/j.margeo.2009.09.011.
Marmorino, G. O., G. B. Smith, and W. D. Miller (2013), Infrared remote sensing of surf-zone eddies, *IEEE J. Selec. Top. Appl. Earth Obs. Remote Sens.*, *6*(3, SI), 1710–1718, doi:10.1109/JSTARS.2013.2257695.
McLachlan, A., and A. Brown (2010), *The Ecology of Sandy Shores*, Elsevier Sci.
Noble, M., B. Jones, P. Hamilton, J. Xu, G. Robertson, L. Rosenfeld, and J. Largier (2009), Cross-shelf transport into nearshore waters due to shoaling internal tides in San Pedro Bay, CA, *Cont. Shelf Res.*, *29*(15), 1768–1785, doi:10.1016/j.csr.2009.04.008.
Omand, M. M., J. J. Leichter, P. J. S. Franks, A. J. Lucas, R. T. Guza, and F. Feddersen (2011), Physical and biological processes underlying the sudden appearance of a red-tide surface patch in the nearshore, *Limnol. Oceanogr. Methods*, *56*, 787–801.
Omand, M. M., F. Feddersen, R. T. Guza, and P. J. S. Franks (2012), Episodic vertical nutrient fluxes and nearshore phytoplankton blooms in southern California, *Limnol. Oceanogr. Methods*, *57*(6), 1673–1688, doi:10.4319/lo.2012.57.6.1673.
Peregrine, D. H. (1998), Surf zone currents, *Theor. Comput. Fluid Dyn.*, *10*, 295–309.
Pineda, J. (1991), Predictable upwelling and the shoreward transport of planktonic larvae by internal tidal bores, *Science*, *253*(5019), 548–551, doi:10.1126/science.253.5019.548.
Pineda, J. (1994), Internal tidal bores in the nearshore: Warm-water fronts, seaward gravity currents and the onshore transport of neustonic larvae, *J. Mar. Res.*, *52*(3), 427–458, doi:10.1357/0022240943077046.
Polzin, K., J. Toole, J. Ledwell, and R. Schmitt (1997), Spatial variability of turbulent mixing in the abyssal ocean, *Science*, *276*(5309), 93–96, doi:10.1126/science.276.5309.93.
Putrevu, U., and I. A. Svendsen (1993), Vertical structure of the undertow outside the surf zone, *J. Geophys. Res.*, *98*, 22,707–22,716, doi:10.1029/93JC02399.
Reniers, A., E. Thornton, T. Stanton, and J. Roelvink (2004), Vertical flow structure during Sandy Duck: Observations and modeling, *Coastal Eng.*, *51*(3), 237–260, doi:10.1016/j.coastleng.2004.02.001.
Reniers, A. J. H. M., J. H. MacMahan, E. B. Thornton, T. P. Stanton, M. Henriquez, J. W. Brown, J. A. Brown, and E. Gallagher (2009), Surf zone surface retention on a rip-channeled beach, *J. Geophys. Res.*, *114*, C10010, doi:10.1029/2008JC005153.
Rippy, M., P. Franks, F. Feddersen, R. Guza, and D. Moore (2013), Factors controlling variability in nearshore fecal pollution: The effects of mortality, *Mar. Pollut. Bull.*, *66*(12), 191–198, doi:10.1016/j.marpolbul.2012.09.003.
Ruessink, B. G. (2010), Observations of turbulence within a natural surf zone, *J. Phys. Oceanogr.*, *40*(12), 2696–2712, doi:10.1175/2010JPO4466.1.
Schiff, K. C., M. J. Allen, E. Y. Zeng, and S. M. Bay (2000), Southern California, *Mar. Pollut. Bull.*, *41*, 76–93.
Smart, P. L., and I. M. S. Laidlaw (1977), An evaluation of some fluorescent dyes for water tracing, *Water Resour. Res.*, *13*, 15–33.
Smith, J., and J. Largier (1995), Observations of nearshore circulation: Rip currents, *J. Geophys. Res.*, *100*, 10,967–10,975, doi:10.1029/95JC00751.
Spydell, M., F. Feddersen, R. T. Guza, and W. E. Schmidt (2007), Observing surfzone dispersion with drifters, *J. Phys. Oceanogr.*, *27*, 2920–2939.
Spydell, M. S., F. Feddersen, and R. T. Guza (2009), Observations of drifter dispersion in the surfzone: The effect of sheared alongshore currents, *J. Geophys. Res.*, *114*, C07028, doi:10.1029/2009JC005328.
Talbot, M., and G. Bate (1987), Rip current characteristics and their role in the exchange of water and surf diatoms between the surf zone and nearshore, *Estuarine Coastal Shelf Sci.*, *25*(6), 707–727.
Winant, C. (1974), Internal surges in coastal waters, *J. Geophys. Res.*, *79*, 4523–4526, doi:10.1029/JC079i030p04523.
Wong, S. H. C., A. E. Santoro, N. J. Nidzieko, J. L. Hench, and A. B. Boehm (2012), Coupled physical, chemical, and microbiological measurements suggest a connection between internal waves and surf zone water quality in the Southern California Bight, *Cont. Shelf Res.*, *34*, 64–78, doi:10.1016/j.csr.2011.12.005.